Using radar altimeter backscatter to evaluate ice cover on the Yukon River

Research Thesis

Presented in partial fulfillment of the requirements for graduation
with Research Distinction in Earth Sciences in the undergraduate colleges of
The Ohio State University

by

Stephen P. Coss

The Ohio State University

August 2015

Project Advisor: Professor Michael T. Durand, School of Earth Sciences

Table of Contents

Abstract....ii
Acknowledgments....iii
List of Figures....iv
List of Tables....iv
List of Equations....iv
Introduction....1
Objectives....2
Study Area....3
Data....5
Methods....9
Results....13
Discussion....15
Conclusions....20
Recommendations for future work....21
References....22
Appendix....A1

Abstract

Use of radar altimetry for measuring fresh water systems is a blossoming area of research that has great potential to develop science's understanding of this precious human resource. The field of satellite altimetry has benefitted from enormous gains since the 1970s. With the launch of GEOS 3 in 1975, humanity began a quest to achieve an understanding of the hydrosphere on a scale previously thought impossible. Though historically the focus of altimetry missions has been studying the ocean, hardware advances have allowed use of satellite altimetry at much higher resolutions, making study of inland waters a possibility. One underlying challenge is to establish a reliable way to determine whether an altimeter is measuring the intended target when used for inland study; surface water measurement, for instance, is confounded by ice coverage, particularly at high latitudes. To overcome this obstacle, Landsat satellite imagery was used to isolate Jason-2 altimetry data from the Yukon River. An altimeter measurement of radar backscatter (how much of the original signal was collected after surface reflection), σ_0, was extracted from the Jason-2 data set, while relative ice cover was determined visually from the Landsat image. σ_0, or the backscatter coefficient, is a metric for the portion of the original radar signal that is returned to the satellite. Water typically returns a much higher reading than ice or land. By manually matching relative ice cover to measured σ_0 values, we propose to create a standard curve for σ_0, with the long term goal of automating the process of determining relative ice cover by removing the need for direct observation. While this project has had promising findings and has identified a traceable seasonal pattern in σ_0, we have demonstrated that to determine a one- to-one relationship between ice and backscatter will be challenging.

Notable findings include that there were no scenes without complete ice cover with σ_0 readings below 8.6dB. The mean σ_0 reading during ice cover was 17.6dB, with a standard deviation of 8.67 dB. The data were highly skewed toward lower end of the range, but had a lengthy tail of measurements that extended well into σ_0 values that would be expected from liquid water. The majority of data from fully frozen scenes is grouped around 13.3 dB. In fact 72% of the data fell within one standard deviation of that value. In the case of completely thawed scenes, the mean value was 37.08 dB, with a standard deviation of 10.07 dB. This grouping is not very tight making a confident classification based only on σ_0 difficult. . Melting ice frequently resembles water in terms of its backscatter signature while maintain enough coverage to obstruct hydrologically valid measurements. A seasonal pattern in σ_0 has been observed, though it is not yet well enough defined to be used for ice classification

Acknowledgements

First and foremost I would like to thank my advisor Mike Durand for giving me the opportunity to work with him and his research group. I would also like to thank everyone else involved in the measurements group—C.K. Shum, Chan Yi, Yuanyuan Jia, Qi Guo, and Steve Tuozzolo. Without the insight and skills of the members of this group, none of this research would have been possible. I would like to thank the NASA MEASURES group and P.I. Dennis Lettenmaier (UCLA) for providing the primary source of funding to our project (grants NNX13AK45A, and NNX15AH05A) and for their collaborative efforts. I would also like to thank the School of Earth Sciences for awarding me the Susie L. Shipley Undergraduate Scholarship and the Arts and Sciences Honors Committee for awarding me the Honors Research Scholarship. These funds made my undergraduate career and this project financially accessible. I would like to thank the USGS Landsat program for the use of their imagery. Open source Satellite images are an invaluable public resource. I would also like to thank NASA and the Ocean Surface Topography Mission, Jason-2. It is only through access to the enormous and continually expanding data from this mission that research of this kind is made possible. I would like to thank the Byrd Polar and Climate Research Center for access to their resources. I would especially like to thank Tom Kassebaum. Tom kept me up and running through all of my hardware struggles often dedicating hours of his time. Lastly, and most importantly, I would like to thank the faculty in the School of Earth Sciences. You are an amazing group of educators that have a level of pride in your work that is rare to find in almost any circumstance. Many of you have gone beyond the limits of your duty time and time again to improve the lives of your students, including me.

List of Figures

1. Map showing the extent of the Yukon River Basin
2. Locations of USGS Pilot Station, and Yukon station 5
3. The Landsat scenes, virtual station locations and Jason-2 Ground tracks used in the study
4. Example "Virtual Station" with Jason-2 footprint center points from 1 cycle
5. Example Scenes that fit each classification used in the study
6. a) USGS height (mean difference subtracted) and Jason-2 height time series over the Jason-2 mission period, b) Jason-2 σ_0 time series over the Jason-2 mission period
7. A histogram of σ_0 Values across all years and stations for all three classifications
8. Station 5 average σ_0 with corresponding images
9. Landsat scenes from a) April 4 2009, b) April 20 2009, c) May 6 2009, d) July 1 2009 e) May 14 2009, f) May 30 2009, g) August 10 2009

List of Tables

1. QA/QC flags used when extracting data from the GDR
2. Percentage of cycles having data and up flow distance for Virtual Stations used in the study
3. Data from the images in Figure 9

List of Equations

1. The formula for σ_0

Introduction

The primary requirement for life on Earth is water. Before food, shelter, or energy, humanity requires fresh water to live. With an increase in fresh water needs being exacerbated by climate change and sea level rise, the growing human population has never experienced a more critical need for accounting of fresh water resources. Many parts of the world are on a path to experience increased water scarcity; already over a third of the world's population is undersupplied with clean water (Gleick, 2003). Although information about surface water is known to be critical for human sustainability, its understanding continues to be poorly constrained, due largely to the limits of the global stream gauge network and limitations in the sharing of data collected in traditional ways (Pavelsky et al., 2014).

Long before scarcity of fresh water seemed an imminent threat, the world's scientists longed for a deep understanding of the hydrosphere on a global scale. In 1975, with the launch GEOS 3, their goals received a huge boon. Radar altimetry would allow unprecedented access to information about ocean circulation and sea-level. For the first time ever, researchers could make observations, not just from a few locations, but from a comprehensive full system viewpoint. Altimetry missions have traditionally been focused on ocean measurements, and reasonably so. It has been through painstaking efforts and countless trials that these methods have been honed enough to even consider other uses. The ability of the science and hardware to advance dramatically, means that we are now entering a new age for satellite altimetry; one where observations are possible at much higher resolutions than were ever thought possible when the first missions were proposed. Even more enticing, are the mountains of data that have already been collected. These ocean missions didn't cease to collect data when inland. That data have been kept to the side until very recently, with no certainty they could yield useful information. For surface water measurements, particularly river heights, ice and surrounding topography present obstacles for acquisition of data on the target surface. Ice covered rivers have two primary ambiguities associated with their measurements: river height may not correspond to flow, and height measurements may be inaccurate or inconsistent. At this time, there is no literature attempting to detect river ice using only altimetric methods, though some researchers have demonstrated a relationship between σ_0, radiometer brightness and ice cover over medium and large lakes. Rybushkina et al. (2014) suggested that the methods they used for ice detection on medium size lakes could feasibly be utilized on some of the larger rivers in the world.

Within the volumes of data already collected by current and past altimeter missions, lies a potential key to bridging this gap in our understanding of the hydrosphere. Use of these data could allow for comprehensive flow datasets for rivers world-wide and grant opportunity, not only for higher resolution observation in key locations that otherwise go unmonitored, but also to view larger areas as a complete system, without limitations of manmade borders. Altimeters have already sown bountiful fields of information for making this hydrologic understanding a possibility. Science needs only to develop the tools to reap the harvest.

Objectives

The primary focus of this research is to determine the relationship between σ_0 measurements and ice cover so that measurements of ice will not be considered a part of the river height data that is being compiled. Ice has been noted to show less than half of the backscatter of open water (Legresy et al., 2005). With Jason-2 data showing maximum $\sigma_0$values of 55dB in the region, it is our hypothesis that 25 dB will serve as a reasonable cut-off for ice cover.

Study Area

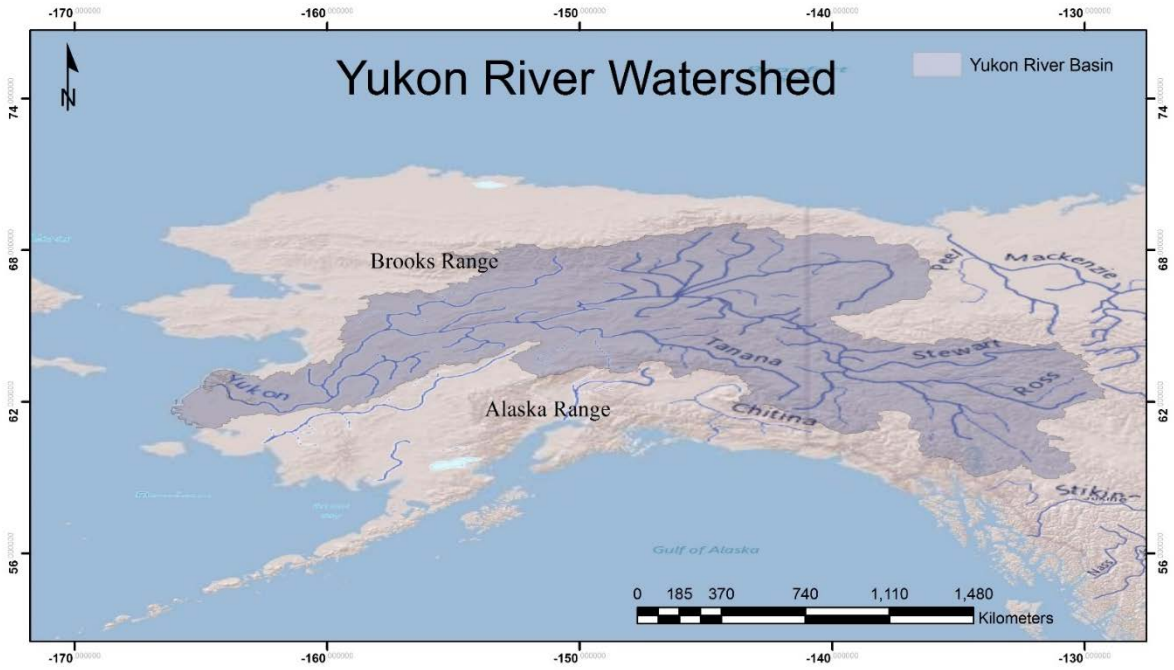

Figure 1 Map showing the extent of the Yukon River Basin

The Yukon River extends 3,190 km from its headwaters in the Atlin District of British Columbia to its mouth in Wade Hampton, Alaska where it drains into the Bering Sea. It has an average instantaneous discharge of 6,430 m^3/s. Its basin spans an impressive 854,700 km^2 across Canada and Alaska, making it over 10% larger than the entire country of Mexico (Brabets et al., 2000). The Yukon River has a fairly regular pattern of freeze-up and break-up. At most locations along the river the first freeze occurs around the 12th of October, and the ice breakup occurs around May 12th with less than six days variation historically (Anon, n.d.) The majority of annual discharge occurs during the summer months and is a result of snow and glacial melt combining with high rainfall. The Yukon is fed by 8 major rivers. The Tanana and White rivers, both of which are glacier fed, contribute 29% of the total flow to the Yukon system. The Yukon deposits 60 million tons of suspended sediment into the Bering Sea annually, while another 20 million tons is estimated to be deposited within its flood plains and braided tributaries (Brabets et al., 2000).

Climate within the Yukon River basin is variable due to the basin's size and the wide range of elevations within. Climate zones have been largely defined by variation in precipitation and temperature (Searby, 1968). The Yukon basin lies primarily within the continental zone, typified by wider range of temperatures than most other zones. It has an average temperature of -6 ºC. The Yukon delta however, is in a transitional zone and has an average temperature of -3 ºC (Brabets et al., 2000). Precipitation within the basin has a wide range and is effectively controlled by topography. Lowland areas receive the least precipitation and can get as little as 25.4 cm annually while mountainous regions can receive as much as 330.2 cm annually. The average precipitation across the basin is 48.26 cm annually. Roughly half of all precipitation in the region occurs as snow between the months of November and March (Brabets et al., 2000). Climate in the region has been changing since about 1840, a trend of warming an average of 0.22ºC/100 years has been observed from 1949-1996 through tree ring, ice breakup, and glacial temperature proxy studies (Brabets et al., 2000).

The mountain ranges of the Yukon are prone to glacier storage. Temperature is the most important factor as alternation between periods of melt and freeze lead to the most rapid exchange from snow to ice (Paterson, 1994). The exceptional conditions in the region have led to 56,327.04 km^2 of the basin's area being glaciated. Glacial capacity for storage and dynamic hydrologic exchange make glaciers a critical and very complicated element of the basin system. The majority of the glaciers in the region are classified as temperate, meaning they have average temperatures of around 0 ^oC (Brabets et al., 2000). The release of water stored in the glacial systems of the Yukon is highly dependent on energy delivered through solar radiation and warm air circulation (Meier, 1969). The temperate status of the ice and the huge quantity of glaciated landscape mean that even small changes in temperature at the right ranges can have intense effect on river discharge.

The Yukon River was chosen as a study area because of its high latitude and size. Latitude is important for two main reasons. Firstly, the altimeter selected has a tight pattern of ground track near Polar Regions. Secondly because of the climate, with nearly eight months annually of ice cover, there is as an abundance of ice measurements to facilitate study. The width of the river was also critical, because the altimeter used was originally designed to be used on the ocean surface and larger fresh water surfaces are more likely to yield viable data.

Data

OSTM/ Jason-2

Launched from the Vandenberg site in California on June 20, 2008, the OSTM(Ocean Surface Topography Mission)/Jason-2 satellite altimeter was designed to establish multidecadal climate records of precise topography measurements (Lambin et al., 2010). The mission continues the record that began in 1992 with TOPEX (Ocean Topography Experiment)/Poseidon and continued in 2001 with Jason-1 (Ménard et al., 2003). Jason-2 boasts substantial gains in precision and accuracy, due largely to its predecessors and the work of investigators studying the data they provided. For that reason, the Ocean Surface Topography Team (OSTST), a joint initiative between the National Aeronautics and Space Administration(NASA), National Oceanic and Atmospheric Administration (NOAA), European Organization of the Exploitation of Meteorological Satellites(EUMETSAT), and the French space agency, The Centre National d'Études Spatiales(CNES), was renewed in 2008 allowing Jason-2 to be staffed with over 300 principal and co-investigators working on 82 approved projects (Lambin et al., 2010).

The OSTM/Jason-2 "level-2" products that are to be provided are altimetric range (satellite to sea surface distance), precise orbit estimation (between 2.7 and 2.9 cm (Flohrer, 2011)), allowing for Jason-2's actual ground track to drift up 2km away from the nominal track , significant wave height, and backscatter coefficient (σ_0)(Lambin et al., 2010). These data are available from both 1 and 20 Hz frequency, where 1 or 20 readings are included per flight second. The on-board altimeter has three primary elements. First, Poseidon-3, a dual frequency (Ku/C bands) radar altimeter provided by CNES, measures the altimetric range, or distance between the instrument and surface at nadir and provides propagation delay correction information. Second, an AMR (Advanced Microwave Radiometer), provided by NASA/JPL (Jet Propulsion Laboratories), provides wet troposphere propagation delay information, needed for altimeter correction of range data. Finally, a three way system for precise orbit determination, which includes the Doppler Orbitography and Radiopositionning Integrated by Satellite (DORIS(supplied by CNES)), a GPS receiver the Global Positioning System Payload (GPSP) and a Laser Retroflector Array (LRA), provided by NASA (Lambin et al., 2010). This system allows for precise location within World Geodetic System 1984 (WGS 1984) so that the ranges measured can be subtracted from the altimeter's height above the Earth Gravitational Model (EGM 2008) geoid to generate a surface height.

Continuing the flight pattern established by TOPEX/Poseidon and Jason-1, OSTM/Jason-2 will use the same repeat track on a nonsus- synchronous orbit, with a 66° incline (meaning that 66°N is the highest latitude the orbit crosses) at an altitude of 1,336km. Cycle length is approximately 10 days. Adjacent tracks are separated by approximately 300km at the equator. The high altitude of the orbit allows for more precision in orbit determination, due to a decrease in the effect of atmospheric drag and Earth's gravitational field (Lambin et al., 2010).

One of the primary directives of the OTSTM/Jason2 mission is to contribute to climate monitoring and understanding. Specific goals lie with creating records of global mean sea level rise, mean dynamic topography and mean global circulation, internal to decadal variability of large-scale circulation, eddy processes, eddy response to climate variations, and coastal and inland water levels. Inland use has primarily been limited to projects involving large lakes, such as the United States Department of Agriculture (USDA) Global Reservoir and Lake Monitor (GRLM), where Jason-2 allowed for several enhancements to previous data. An increase of ~65% in the number of

reservoirs in the specific regions of interest (a total of 39 reservoirs in India, Iraq, Iran, Turkey, Brazil, Argentina, and Australia) was made possible with utilization of the Jason-2 dataset, which showed much better acquisition over smaller, calmer lakes, areas where Jason-1 had a known issue with rejecting data based on on-board filtering (Birkett et al., 2011).

Jason-2 observations provide consistent information over large water surfaces, which will be critical for monitoring global water cycles and variations. Measurements for OSTM/Jason-2 may also shed light on long-term trends that may be due to decadal climate variation, global warming, or local human-induced factors. Retracking algorithms for Jason-2 make it more capable of generating this information than its predecessors (Lambin et al., 2010).

σ_0 , or radar backscatter, is a Jason-2 data set critical to understanding the qualities of the material within the altimeter's radar footprint. It is a quantitative evaluation of the amount of radar signal that is returned to the altimeter.

$$\sigma_0 = \frac{(4\pi)^3 R^4}{t_\lambda^2 G_0^2 \lambda^2 A_{eff} P_t} P_r \quad (1)$$

Equation 1 is the formula for σ_0 presented in Chelton et al. (2001), where R is the satellite altitude, t_λ is the atmospheric transmittance, G_0 is the boresight antenna gain, λ is the wavelength of the electromagnetic radiation transmitted, A_{eff} is the effective footprint area, P_t is the power transmitted, and P_r is the returned power. Because all of the quantities in the multiplicative factor on the right side of the equation are known parameters in the system, or can be determined from the measurement geometry, returned power P_r and therefore σ_0 depend only on the radar scattering characteristics of the area being targeted (Chelton et al., 2001). This metric has been used in traditional ocean focused altimetry studies as a proxy for near-surface wind speed, but has many other potential applications.

Landsat Archive

Starting in 1972 the Landsat Missions have generated an archive of satellite imagery that has provided Scientists an unparalleled record of the status and dynamics of Earth (Cohen and Goward, 2004). Frequently, Landsat data provides our only source for knowledge on critical areas of research like a growing population, climate change, and demand for resources (Wulder et al., 2008). This continually expanding resource has nearly limitless application. Control of the program has had a long and fascinating history of being passed between different agencies and even the private sector. It has passed from NASA, to NOAA, to EOSAT and space imaging corporations (private companies), to the Air Force, and back to NASA and USGS by 1999 where it has remained, though there are plans for Landsat 9 to be led fully by USGS efforts (Wulder et al., 2012).

In 2008, due to a data policy change, all USGS Landsat data held and generated in the future became freely available over the internet to any user (Woodcock et al., 2008). The positive impact that this decision has had on the scientific community is almost hard to fathom in terms of generating study. For example, USGS's EROS (Earth Resource Observation Center) distributed 25,000 Landsat images in 2001, at the price of $600, while 2011 saw the distribution of over 2.5 million free Scenes (Wulder et al., 2012).

For the purpose of this research, images from Landsat missions 4, 5, 7 and 8 were used. Landsat4 (1982-2001) and Landsat5 (1984-3013) were both equipped with MSS (Multispectral Scanner) and TM (Thematic Mapper) sensors, allowing for image resolutions of 30-meters in green to near infrared as well as SWIR (Short Wave Infrared) and 120-meters resolution for thermal infrared. Landsat 7 (launched 1999) and Landsat 8 (launched 2013) are both operational. Landsat 7 is equipped with an ETM+ (Enhanced Thematic Mapper+) sensor, allowing for 30-meter resolutions in visible, near-IR, and SWIR. It is also capable of providing 60-meter resolution images in thermal band, and 15-meter resolution in panchromatic band which is used for sharpening the images. Landsat 8 with an OLI (Operational Landsat Imager) provides data from 9 shortwave and 8 spectral bands at 30-meter resolution as well as panchromatic data at 15-meter resolution. Improved radiometric performance has been achieved with new costal, aerosol, and cirrus bands. Landsat 8 is also equipped with TIRS (Thermal Infrared Sensor) with two long wave thermal bands at 100 meter resolution which are delivered to the OLI for processing allowing all Landsat 8 output data to be at a 30 meter resolution and 16 bit range (USGS, 2013). Since Landsat 4, Landsat missions have had 185km wide swaths in their descending orbit and have orbited the Earth at 705 km altitude. They complete an orbit every 99 minutes, allowing for nearly 14 full orbits a day, with a resultant 16 day full earth coverage cycle. Concurrent missions have always been designed to alternate, so that every location on earth within imaging range is covered every 8 days (USGS, 2013). The variety of data available and the sheer size of its archives, make the Landsat program a tool that is nearly invaluable to workers in remote sensing. Free materials for public use, and continuing the programs legacy, are sure to mean nearly unlimited opportunity for future work.

USGS Pilot Station

Established in 2000 as part of an effort to generate process-based water quality assessment data for the Yukon River, Pilot Station is one of 5 fixed USGS monitoring stations in the Yukon River basin. Gage data availability to the public only extends back to October 2007. While 90 other temporary stations have been established in the basin for different studies, only five remain as permanent fixtures (Anon, 2014). The gage is located just over 197 km from the mouth of the Yukon River, in the town of Pilot Station. Stage height (a height above an arbitrary local datum) and discharge data has been available to the public since October 2007, water temperature since October 2014, and air temperature since March 14th 2015. Hydrological data is not reported at this location during times when the river is frozen, which is typically from mid-October to mid-May (Anon, 2015).

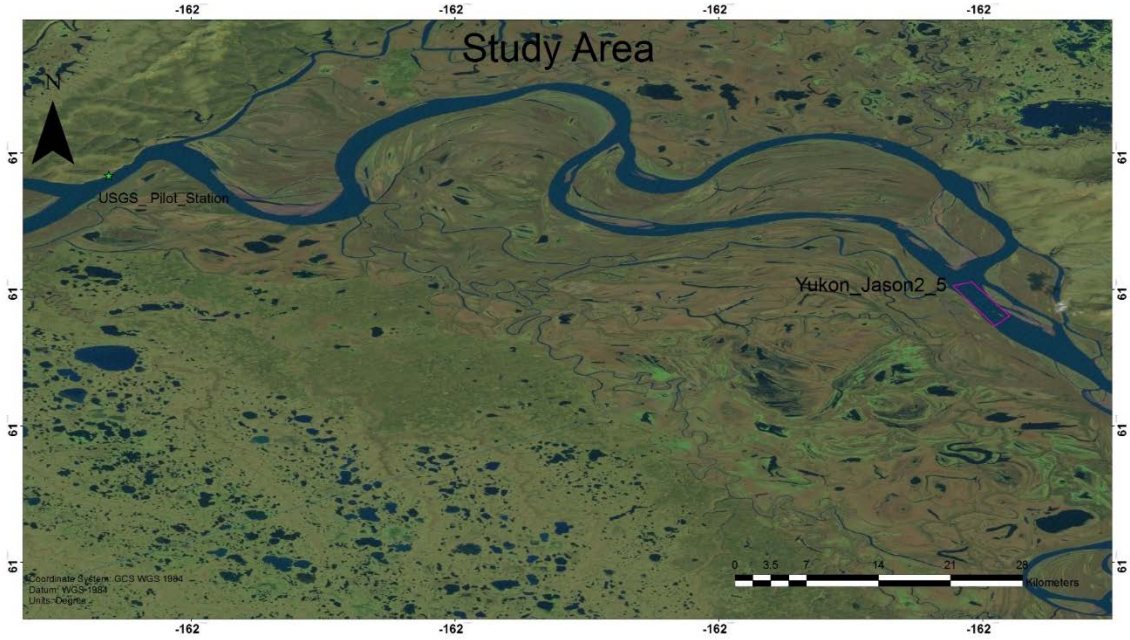

Figure 2 Locations of USGS Pilot Station, and Yukon station 5

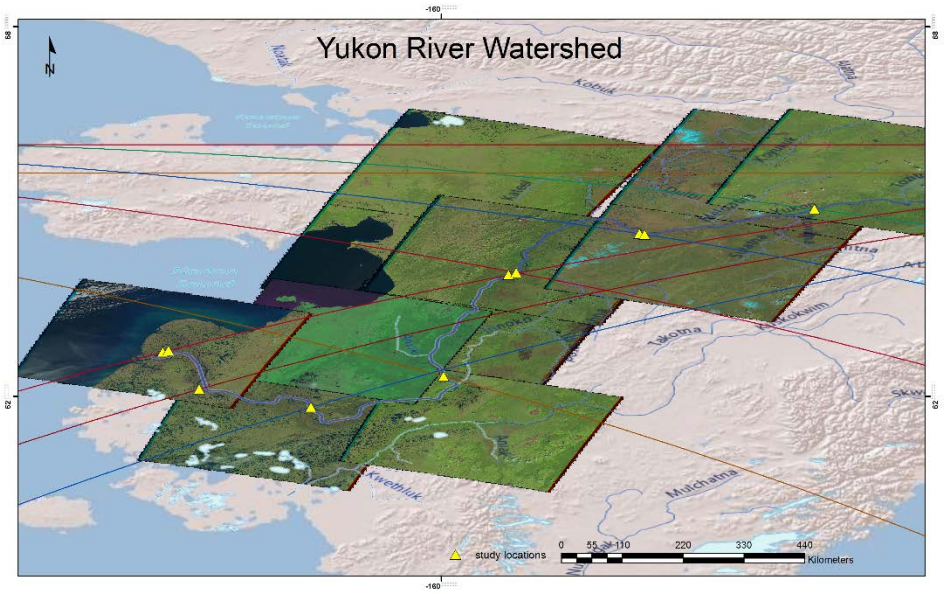

Figure 3 The Landsat scenes, virtual station locations and Jason-2 Ground tracks used in the study

Methods

For the purpose of identification of potential virtual stations(intersections of the Jason-2 ground track and Yukon River), data compiled using RivWidth (Pavelsky and Smith, 2008) was cross-referenced with the ground track for the satellite altimeter Jason-2 to find crossings that lie in sections of the river that are a kilometre or more in width. Landsat scenes were collected for the regions of the river where vertical stations were to be placed. These scenes were the same indicated by the Pavelsky group's NARWidth (Allen and Pavelsky, 2015) database to concur with mean annual discharge. These scenes and the Jason-2 ground track were then compiled so that a shape file of virtual stations could be drawn.

At each crossing of proper width, a polygon with four vertices was drawn at the intersection of the river and the ground track that encompassed the entire width of the river and extended along the river to include a distance of 2 km perpendicular to the nominal ground track to allow for small changes in the actual flight path, which translate into up to ± 2 Km drift in the actual ground track of individual orbit cycles. In total 29 polygons, or virtual stations, were drawn on the Yukon.

Figure 4 Example "Virtual Station" with Jason-2 footprint center points from 1 cycle

The shape file was then processed to extract both the limits of the drawn polygons and the Jason2 ground track associated with each polygon. The Average 20 Hz height and σ_0 data was computed per individual cycle (typically between 3 and 5 individual data points) as seen in figure 4.The Jason2 data from within the boundaries of each polygon was extracted from the GDR, with the following limitations QA/QC flags and using the Ice1 retracker.

Table 1 QA/QC flags used when extracting data from the GDR

1-Hz	20- Hz
Flag orbit_state_flag_rest = 3 (adjusted preliminary/precise orbit)	Altitude alt_20hz is available
Range correction model_dry_tropo_corr is available	Ku band altimeter range (ice retracking) ice_range_20hz_ku is available
Range correction model_wet_tropo_corr is available	Flag ice_qual_flag_20hz_ku = 0 (good, Ku band ice retracking quality)
Range correction iono_corr_gim_ku is available	Ku band backscatter coefficient (ice retracking) ice_sig0_20hz_ku is available and not negative (in dB)
Range correction solid_earth_tide is available	
Range correction pole_tide is available	
The number of 20-Hz data points to be compressed to 1-Hz in a selected pass segment has to be 2 or more.	
The time span of each pass segment should not be longer than 1.5 seconds.	

As a starting point stations that had no data for more than 30% of the cycles of the Jason-2 mission were eliminated because they would not be able to generate a complete time series. σ_0 and river height time series were then generated to establish if the data was a reasonable representation of the river. The most easily verifiable way to eliminate bad data prior to further processing is by height. This is necessary, because the altimeter frequently reports heights that are measurements from surrounding topography when the on-board tracking systems malfunction. Tracking is much more difficult inland, due to the presence of rapid topography changes not present in the open Ocean.

To accomplish this filtering, the data were sorted by first setting an upper and lower cap on viable data at +15m and -10m from median river height. These limits were established with careful consideration of actual USGS gage data of flood and drought events from 105 USGS gages on rivers with watersheds larger than 20,000 km^2. The remaining data was then filtered to remove any values that were below 2m below the 5^{th} percentile of the recorded stage of the river, to correct for artificially low values that are unlikely to represent the river. This can be done in confidence as there should be a gradual decay in low flow outliers when compared to high flow outliers (Steve Tuozzolo, personal communication, June 29, 2015). The remaining measurements were used for further study.

After processing the stations, 10 were selected as optimal for further study, due to the high volume of viable data points remaining after height filtering. Having high confidence in the height data was ideal, as ice-cover was the intended focus of the study. While 70% was used as a cut-off, the majority of the stations had above 90% of cycles represented.

Table 2 Percentage of cycles having data and up flow distance for Virtual Stations used in the study

Station ID	Cycles represented [%]	Up Flow Distance [km]
Yukon_Jason2_0	92	19
Yukon_Jason2_1	93	27
Yukon_Jason2_4	91	114
Yukon_Jason2_5	93	225
Yukon_Jason2_8	88	445
Yukon_Jason2_11	93	660
Yukon_Jason2_13	70	669
Yukon_Jason2_18	90	885
Yukon_Jason2_19	91	860
Yukon_Jason2_21	88	1008

For each Virtual Station selected, Landsat Scenes were collected for the entire mission history of Jason2 (June 20, 2008-present). These images were then inspected manually and given a 1, 2 or 3 classification based on the ice cover shown in the image. A value of 1 was given only when the river was completely ice covered allowing for ice bridging (ice wedged from shore to shore

above the actual water surface), as the measured height no longer represents the water surface, and therefore has no value for hydrological evaluation. A value of 2 was given when ice was clearly

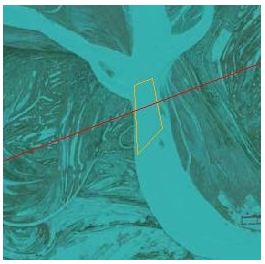		
Classification 1	**Classification 2**	**Classification 3**

Figure 5 Example Scenes that fit each classification used in the study

present, but the edges or more had started to break up, meaning that bridging was not possible and the readings could once again correspond to flow. Class 2 was also critical because these readings were sure to be difficult to differentiate in terms of σ_0 and represent a pivotal transitional phase. The third classification was given only when there was no ice in the virtual station at the time of the image.

The Landsat image dates and ice classifications were then matched to closest fit data from Jason-2, resulting in σ_0 values known to be associated with one of the three ice characteristics. The σ_0 data was put into three groups that included data from all dates and locations studied, with the hope that a clear, broadly applicable pattern might emerge.

Results

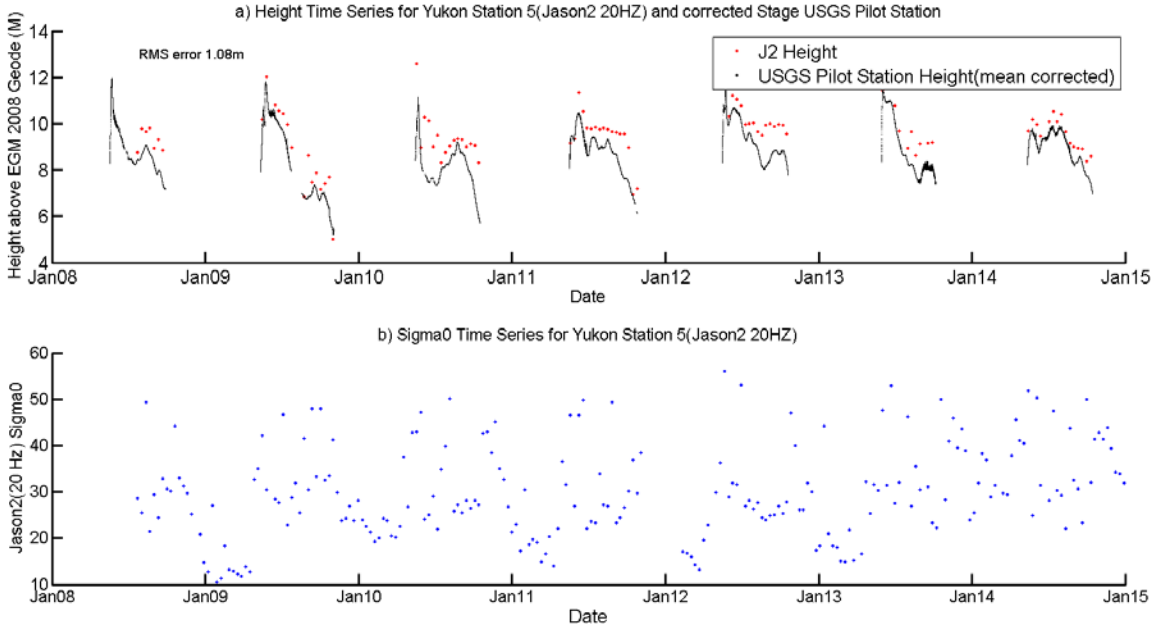

Figure 6 a) USGS height (mean difference subtracted) and Jason-2 height time series over the Jason-2 mission period, b) Jason-2 σ_0 time series over the Jason-2 mission period

Figure 6a shows the average river height time series for virtual station 5 on the Yukon, as well as the height corrected (mean difference added) stage of USGS Pilot Station. The Jason-2 heights from times that USGS is not reporting have been removed, from both to ease comparison, and because the data from these times, when viewed, clearly does not accurately represent the river surface. The Jason-2 height data represents the river quite accurately (1.08m root mean squared error). In Figure 6b(Jason-2 σ_0) has been set to the same x axis to demonstrate that σ_0 typically hits its minimum whilst USGS is not reporting data due to ice cover, showing strong correlation with

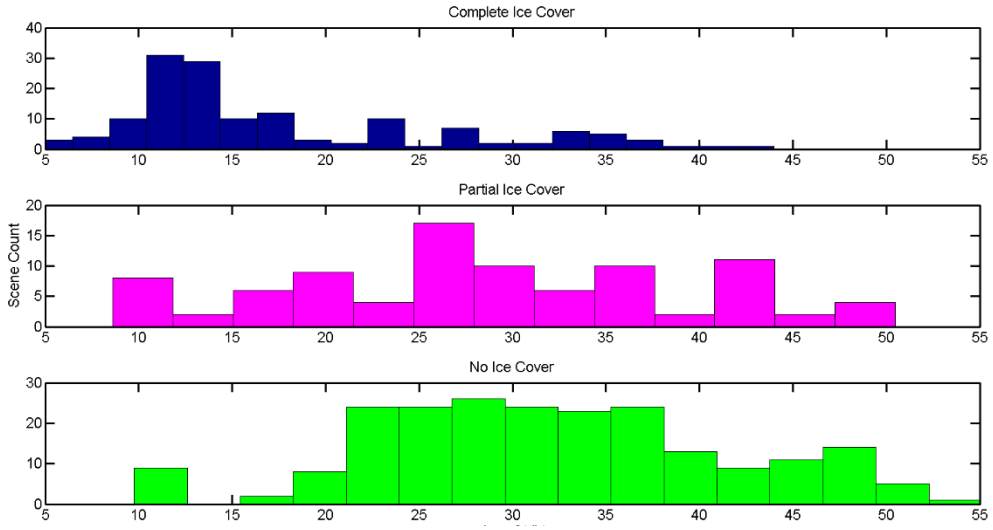

Figure 7 A histogram of σ_0 Values across all years and stations for all three classifications

low σ_0 values and Observed ice cover. There are other USGS data gaps that are not likely to be associated with ice, such as mid-2009. These occur because of log jams or other obstructions, heavy sediment, or malfunctioning equipment.

Figure 7 is a histogram across all years and stations and demonstrates that the data has significant ice and σ_0 correlation, in terms of the three previously mentioned classifications for Landsat images. One notable observation, is that there are no scenes without complete ice cover that fall below 8.6db. The mean frozen σ_0 is 17.6 dB, with a standard deviation of 8.67 dB due to a lengthy tail that extends up to 43.9 dB. The class 1 (completely frozen) scene data had a range of over 39 dB. The tight grouping around 13.30db in ice values is promising. 72% of all of the ice data fell within a standard deviation of that value. The mean value for partially thawed images was 28.62 dB, with a standard deviation of 10.70 dB. The partially thawed data spanned a nearly 42 dB range. The mean value for thawed scenes was 32.08 dB, with a standard deviation of 9.66 dB. The fully thawed data had an over 48 dB range. It is also important to note the anomalously low σ_0 values in the thawed data. The grouping that is isolated around in 10dB is all from one station (station 21) with a particularly pronounced bar that is exposed during lower flow. The phenomenon is explained further in the discussion section. When attempting to isolate the groups it is notable that 28.7 % of the fully frozen data lies above 20 dB, while only 6% of thawed data falls below that same limit. There is, however, no clear dividing line between partial ice values and the two end members. Partial ice cover values span nearly the entire range of the combined data set, making distinction between the three quite difficult.

Discussion

It is clear when examining images and their corresponding σ_0 values that ice and low σ_0 have high correlation. However, distinct and easily discernible groupings that we hypothesized would be visible, never immerged. To examine this phenomenon further, a virtual station was selected that could be easily verified by comparison to a physical streamgage. Virtual station 5 was selected because of its proximity (within 73 km) to the USGS gage at Pilot Station. 2009 was selected from a complete collection of Landsat images showing station 5 during the length of the Jason-2 mission, as a year exemplifying both expected σ_0 correlation and discrepancies. The additional scenes from the set are available as an appendix to this document.

Figure 8 is a detailed look at Jason-2 σ_0 data from 2009. The average value has been plotted with error bars showing the minimum and maximum measurements from the time the average was taken. The plot has been overlain with images from station 5 to demonstrate how ice cover and σ_0

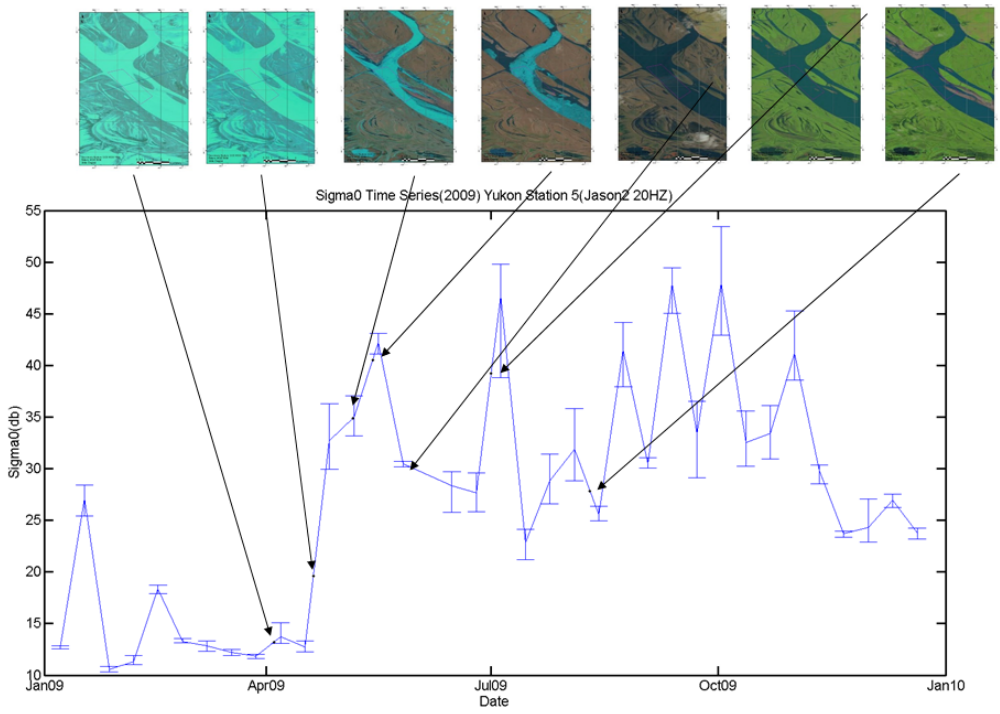

Figure 8 Station 5 average σ_0 with corresponding images

are related. While several of the images show the expected pattern of melt corresponding with a rise in average σ_0, several are in clear violation. One of the highest values is during partial ice cover in May 2009 (42.44dB). The reading in August (25.30 dB) is much lower than might be expected for open water when compared with other data from this location.

a) 4.4.2009-(13.18 dB)

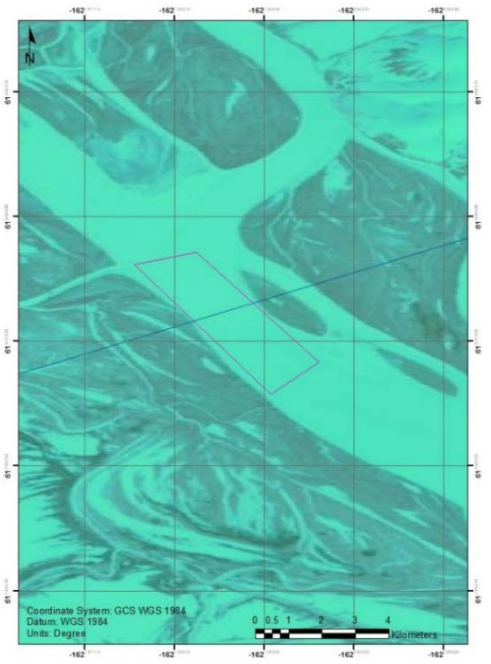

b) 4.20.2009-(12.25dB)

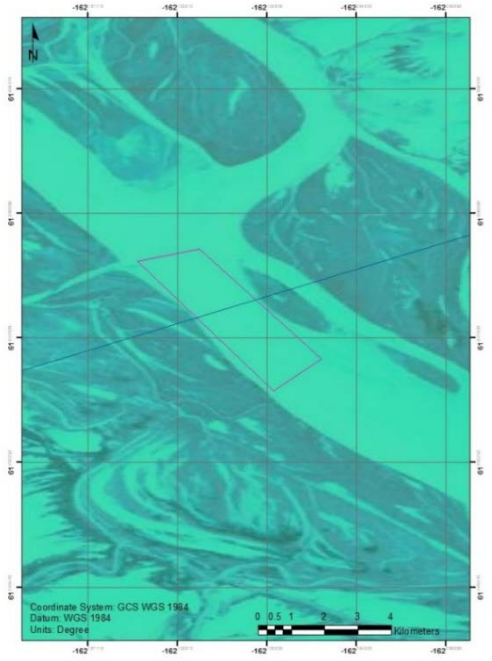

c) 5.6.2009-(33.15dB)

d) 7.1.2009-(49.04dB)

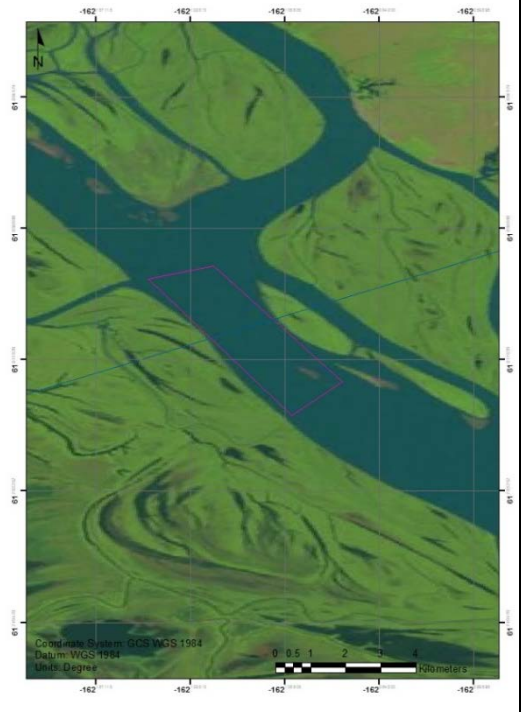

e) 5.14.2009-(42.44dB)

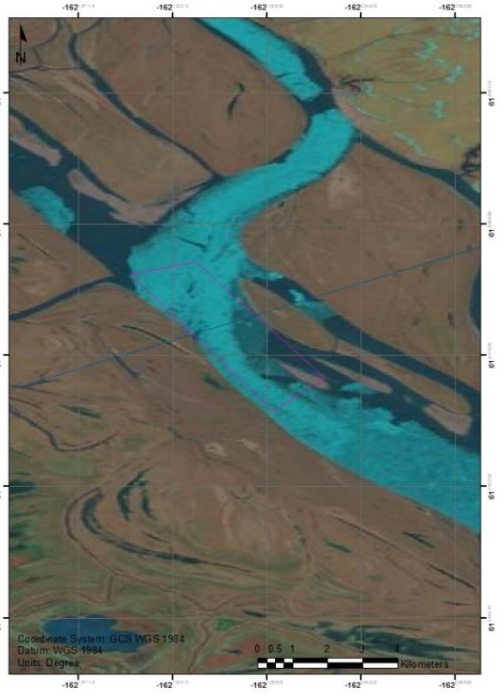

f) 5.30.2009-(30.5dB)

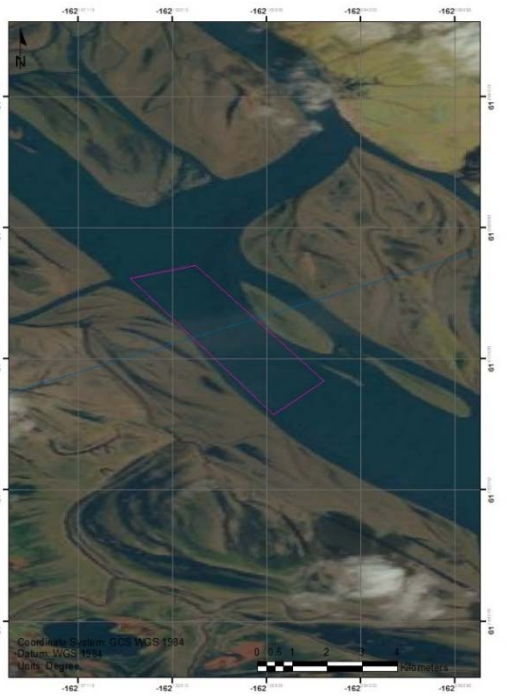

g) 8.10.2009-(25.3dB)

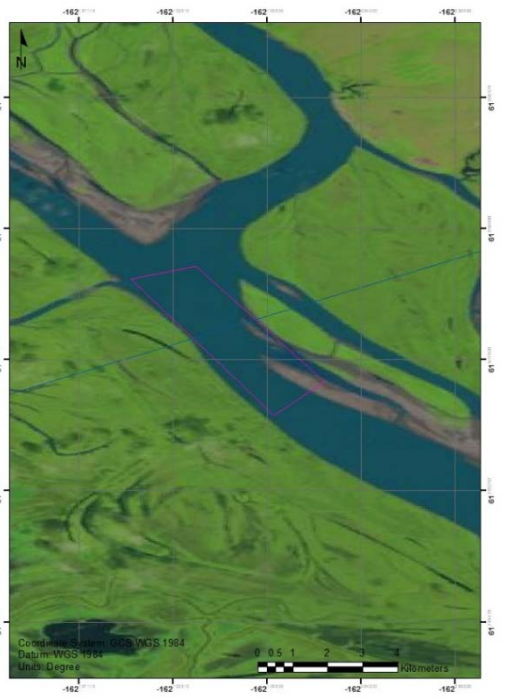

Figure 9 Landsat scenes from a) April 4 2009, b) April 20 2009, c) May 6 2009, d) July 1 2009 e) May 14 2009, f) May 30 2009, g) August 10 2009

Table 3 Data from the images in Figure 9

Figure Number	Landsat Date	USGS Height(mean difference subtracted) [m]	Jason-2 Date	Jason-2 average height [m] Above EGM 2008 geoid	Jason-2 average σ_0 [dB]
9a	4 April 2009	Not reported	6 April 2009	5.23	13.18
9b	20 April 2009	Not Reported	16 April 2009	7.59	12.25
9c	6 May 2009	Not Reported	6 May 2009	6.83	33.15
9d	1 July 2009	7.17	4 July 2009	7.75	49.04
9e	14 May 2009	6.09	16 May 2009	7.60	42.44
9f	30 May 2009	8.13	26 May 2009	9.46	30.50
9g	10 August 2009	Not Reported	13 August 2009	7.25	25.30

Figure 9 is collection of Landsat images from 2009. The images in figure 9a-d show the continuously observed pattern of σ_0 increasing as surface ice decreases. Figure 9a and 9b have values around 13dB, well within the range expected for fully frozen backscatter values. Figure 9c demonstrates a transition towards the thawed end of the spectrum. At 33.15 dB the σ_0 value is above what would be expected for a fully frozen scene, but is still relatively low, a reflection of the large amount of ice still present. Finally Figure 9d has a distinctly high average σ_0 due to its lack of ice cover.

The images selected for Figure 9e-g were chosen because they seem to violate the seasonal pattern that is expected. Figure 9e has an average σ_0 that is high for having ice present. It is possible that this is due to water pooling on the remaining ice's surface, or that in the 2 days between the image and when the Jason-2 pass occurred, the ice was washed away. Figure 9f and 9g should have a higher average σ_0 values. It is possible that the Jason-2 data has been contaminated with measurements from the land surface, which evaded height filtering. This is quite likely for 14c where numerous bars are visibly exposed.

One more element to consider is the presence of snow. Snow can also cause slight variations in σ_0 and is often difficult to identify even when using imagery. As noted by Bevin et al. (1995) surficial snow has unpredictable texture and heightened roughness on the surface could contribute to lower σ_0 measurements. This effect is of course diminished as the snow melts and compacts, reducing the intensity of the surfaces relief. This means that the σ_0 values in this study that were associated with ice cover and were particularly low, could be related to surficial complexity in overlying snow, rather than the underlying ice.

As was demonstrated by this body of research, Sigma0 alone is not a suitable way to reliably determine ice cover. There is, however an observable pattern that is inspiring in terms of further research. Some of the data that seems not to correlate correctly, could be explained by using other metrics such as peakiness. A Pulse Peakiness Parameter, has been shown to be a sensitive detector of non-ocean waveforms associated with contamination of ocean returns (Laxon and Rapley, 1987). The success that Laxon and Rapley achieved is quite promising. Peakiness might be used as an indication of land returns that have erroneously low σ_0, or melt water returns, with erroneously high Sima0 values. Other workers have perused used of radiometer brightness readings at 18.7 and 37 GHz to verify σ_0 readings over large to medium sized lakes. The method was able to reliably determine freeze times quantitatively, and it is suggested by the authors that their method should be viable on large rivers (Rybushkina et al., 2014).

Conclusions

This body of research has clearly shown, that while there is a fascinating correlation between σ_0 and ice, that relationship alone, is not concrete enough to reliably determine ice cover. While is it possible to evade the issue of using an altimeter to determine ice cover by using in-situ gages, observational reporting, or other remote sensing(such as Landsat images), the inquiry remains a valid one. Radar can penetrate cloud cover, doesn't require daylight, and is capable of capturing information where there are no traditionally sourced data. Most importantly, using existing data generated from an altimeter to access the quality of height measurements allows the worker to know that the conditions they are using to reject or accept data existed at the exact moment that they were generated. It is not an ideal situation to discover that a body of research has not revealed a simple solution to the question you yearn to answer, but within this work is a piece of the puzzle, likely one that will be tantamount to solving the problem we set out to resolve.

Recommendations for Future Work

This work has established a basis for using σ_0 to determine ice cover on rivers. Most importantly, it has identified some of the issues in using this method, which might be identified using other resources. A Pulse Peakiness Parameter, has been shown to be a sensitive detector of non-ocean waveforms associated with contamination of ocean returns (Laxon and Rapley, 1987). The success that Laxon and Rapley achieved is quite promising for identification cycles that might contain measurements obscuring ideal σ_0 signature. . Peakiness might be used as an indication of land returns that have erroneously low σ_0, or melt water returns, with erroneously high Sima0 values. Other workers have perused used of radiometer brightness readings at 18.7 and 37 GHz to verify σ_0 readings over large to medium sized lakes. The method was able to reliably determine freeze times quantitatively, and it is suggested by the authors that their method should be viable on large rivers (Rybushkina et al., 2014). It is my hope that one of these available metrics from within the Jason-2 data set will make a primarily σ_0 based river ice detection system viable.

References cited

Allen, G. H., and T. M. Pavelsky (2015), Patterns of river width and surface area revealed by the satellite-derived North American River Width data set, *Geophysical Research Letters*, *42*(2), 395–402, doi:10.1002/2014GL062764.

Anon (2014), Yukon River Basin Studies, *USGS Alaska Science Center*. Available from: http://alaska.usgs.gov/science/program.php?pid=36 (Accessed 12 July 2015)

Anon (2015), USGS Current Conditions for the Nation, *National Water Information System : Web Interface*. Available from: http://waterdata.usgs.gov/nwis/uv?site_no=15565447 (Accessed 12 July 2015)

Anon (n.d.), Alaska-Pacific River Forcast Center, *National Weather Service*. Available from: http://aprfc.arh.noaa.gov/php/brkup/breakupDb.php?riverOption_=Yukon&riverOption__=Yukon+River&riverOption___=Stevens+Village++%2835+yrs%29&riverOption=Yukon+-+Yukon+River+at+Stevens+Village+%28ID%3A493%29 (Accessed 22 June 2015)

Beaven, S. G., G. L. Lockhart, S. P. Gogineni, A. R. Hossetnmostafa, K. Jezek, A. J. Gow, D. K. Perovich, A. K. Fung, and S. Tjuatja (1995), Laboratory measurements of radar backscatter from bare and snow-covered saline ice sheets, *Remote Sensing*, *16*(5), 851–876.

Birkett, C., C. Reynolds, B. Beckley, and B. Doorn (2011), From research to operations: the USDA global reservoir and lake monitor, in *Coastal altimetry*, pp. 19–50, Springer.

Brabets, T. P., B. Wang, and R. H. Meade (2000), *Environmental and hydrologic overview of the Yukon River Basin, Alaska and Canada*, US Department of the Interior, US Geological Survey.

Chelton, D. B., J. C. Ries, B. J. Haines, L.-L. Fu, and P. S. Callahan (2001), Satellite altimetry, *International Geophysics*, *69*, 4-5.

Cohen, W. B., and S. N. Goward (2004), Landsat's role in ecological applications of remote sensing, *Bioscience*, *54*(6), 535–545.

Flohrer, C., M. Otten, T. Springer, and J. Dow (2011), Generating precise and homogeneous orbits for Jason-1 and Jason-2, *Advances in Space Research*, *48*(1), 152–172, doi:10.1016/j.asr.2011.02.017.

Gleick, P. H. (2003), Global freshwater resources: soft-path solutions for the 21st century, *Science*, *302*(5650), 1524–1528.

Lambin, J., Morrow, R., Fu, L., Willis, J., Bonekamp, H., Lillibridge, J., Perbos, J., Zaouche, G., Vaze, P., Bannoura, W., Parisot, F., Thouvenot, E., Coutin-Faye, S., Lindstrom, E., and Mignogno, M. (2010), The OSTM/Jason-2 Mission, *Marine Geodesy*, *33*(sup1), 4–25, doi:10.1080/01490419.2010.491030.

Laxon, S. W., and C. G. Rapley (1987), Radar altimeter data quality flagging, *Advances in Space Research*, *7*(11), 315–318.

Legresy, B., F. Papa, F. Remy, G. Vinay, M. van den Bosch, and O.-Z. Zanife (2005), ENVISAT radar altimeter measurements over continental surfaces and ice caps using the ICE-2 retracking algorithm, *Remote Sensing of Environment*, *95*(2), 150–163.

Meier, M. F. (1969), Glaciers and Water Supply, *Journal (American Water Works Association)*, *61*(1), 8–12, doi:10.2307/41265966.

Ménard, Y., L.-L. Fu, P. Escudier, F. Parisot, J. Perbos, P. Vincent, S. Desai, B. Haines, and G. Kunstmann (2003), The Jason-1 Mission., *Marine Geodesy*, *26*(3/4), 131–146.

Paterson, W. S. B. (1994), 7 – Basal , in *The Physics of Glaciers (Third Edition)*, edited by W. S. B. Paterson, pp. 132–157, Pergamon, Amsterdam.

Pavelsky, T. M., and L. C. Smith (2008), RivWidth: A software tool for the calculation of river widths from remotely sensed imagery, *Geoscience and Remote Sensing Letters, IEEE*, *5*(1), 70–73.

Pavelsky, T. M., M. T. Durand, K. M. Andreadis, R. E. Beighley, R. C. D. Paiva, G. H. Allen, and Z. F. Miller (2014), Assessing the potential global extent of SWOT river discharge observations, *Journal of Hydrology*, *519, Part B*(0), 1516–1525, doi:10.1016/j.jhydrol.2014.08.044.

Rybushkina, G., Y. Troitskaya, and I. Soustova (2014), Remote sensing of water level and ice cover of large and middle-sized lakes of Russia, *Conference on Remote Sensing for Agriculture, Ecosystems, and Hydrology* vol. 9239, pp. 923922–923922–10.

Searby, H. W. (1968), *Climates of the states: Alaska*, US Government Printing Office.

USGS (2013), Landsat: A Global Land-Imaging Mission, Available from: http://pubs.usgs.gov/fs/2012/3072/fs2012-3072.pdf

Woodcock, C. E., R. Allen, M. Anderson, A. Belward, R. Bindschadler, W. Cohen, F. Gao, S. N. Goward, D. Helder, and E. Helmer (2008), Free access to Landsat imagery., *Science (New York, NY)*, *320*(5879), 1011.

Wulder, M. A., J. C. White, M. Cranny, R. J. Hall, J. E. Luther, A. Beaudoin, D. G. Goodenough, and J. A. Dechka (2008), Monitoring Canada's forests. Part 1: Completion of the EOSD land cover project, *Canadian Journal of Remote Sensing*, *34*(6), 549–562.

Wulder, M. A., J. G. Masek, W. B. Cohen, T. R. Loveland, and C. E. Woodcock (2012), Opening the archive: How free data has enabled the science and monitoring promise of Landsat, *Remote Sensing of Environment*, *122*(0), 2–10, doi:10.1016/j.rse.2012.01.010.

Appendix: A

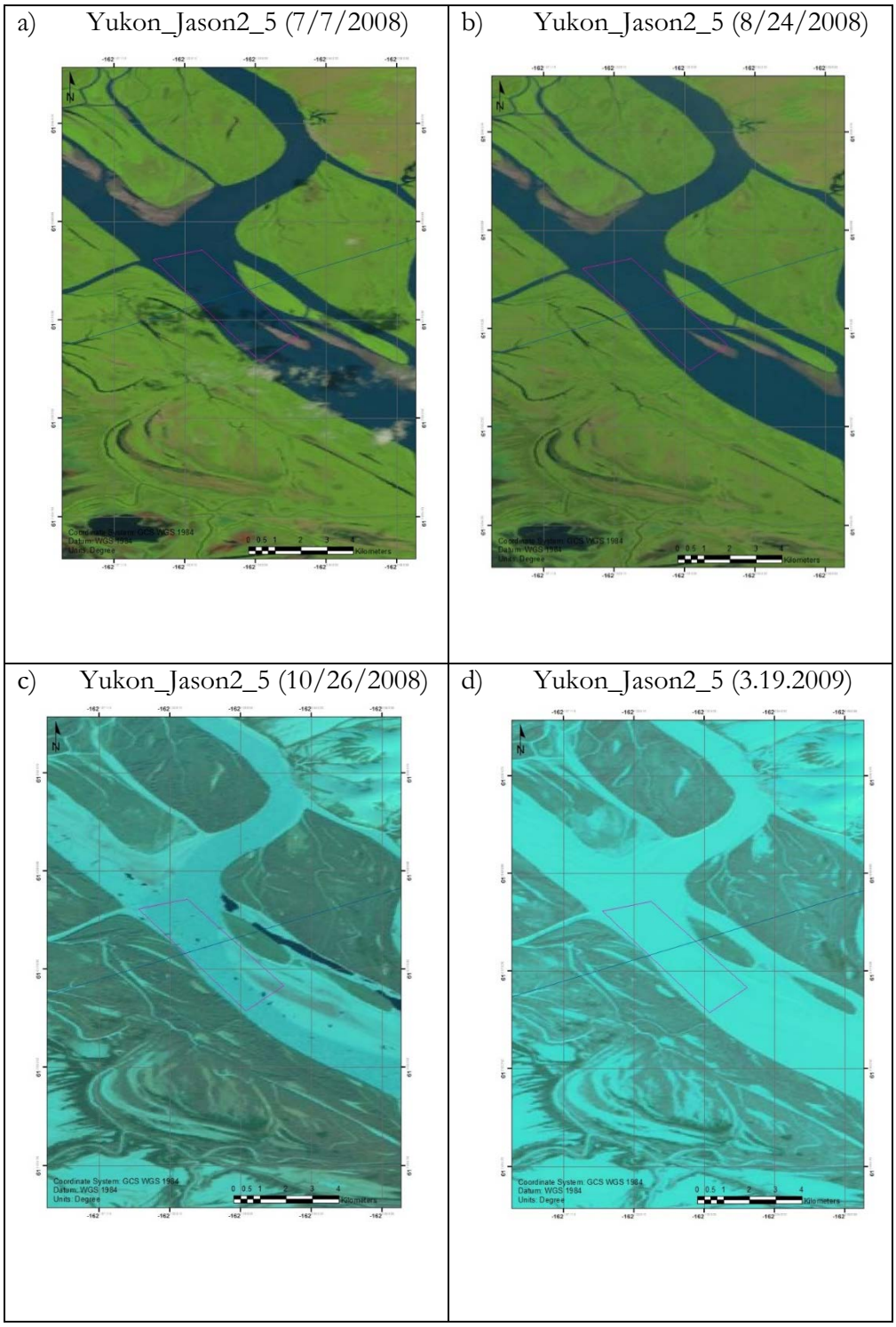

Figure A1. Landsat scenes from a) July 7 2008, b) August 24 2008, c) October 26 2008, d) March 19 2009

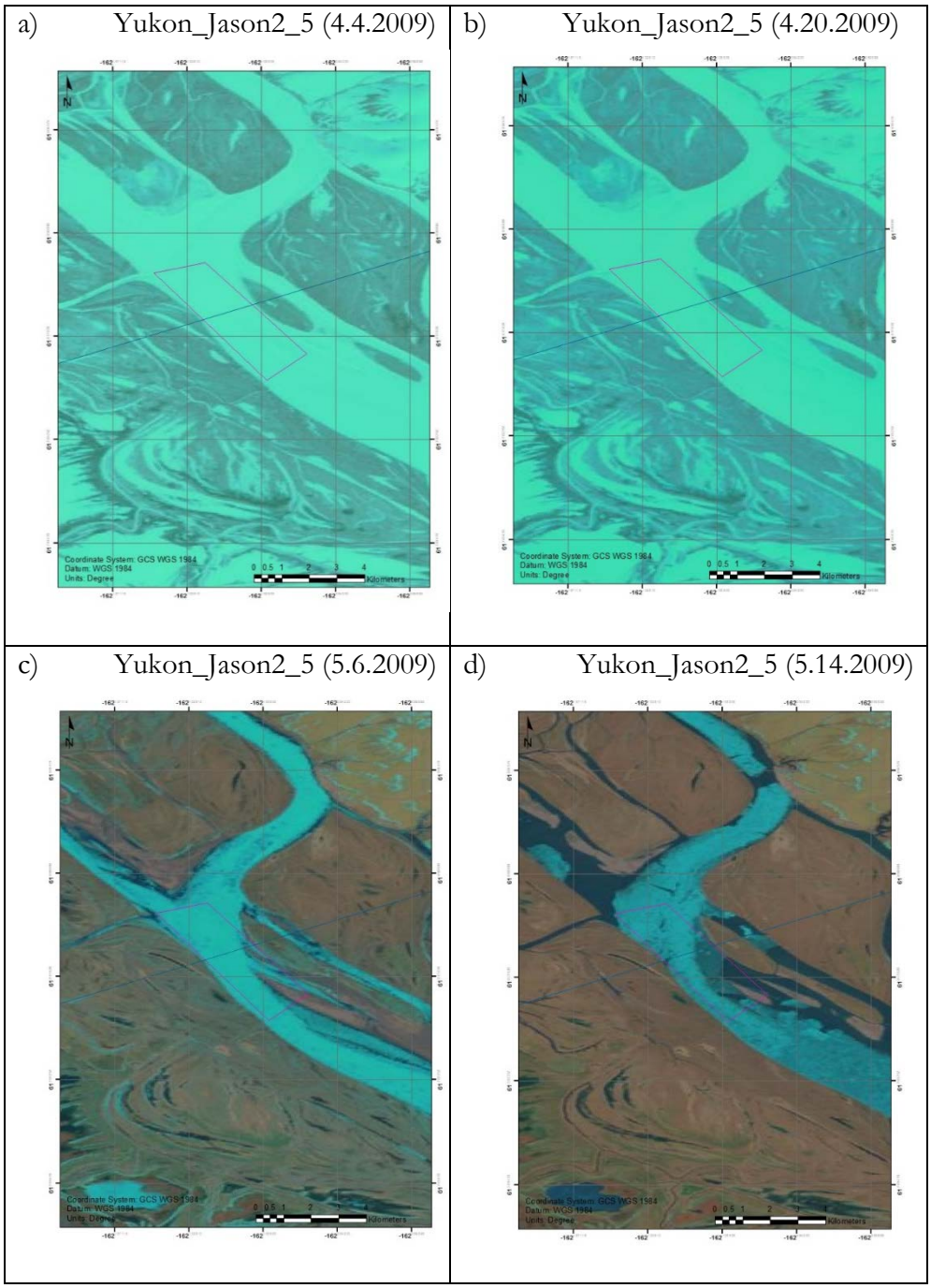

Figure A2 Landsat scenes from a) April 4 2009, b) April 20 2009, c) May 6 2009, d) May 14 2009

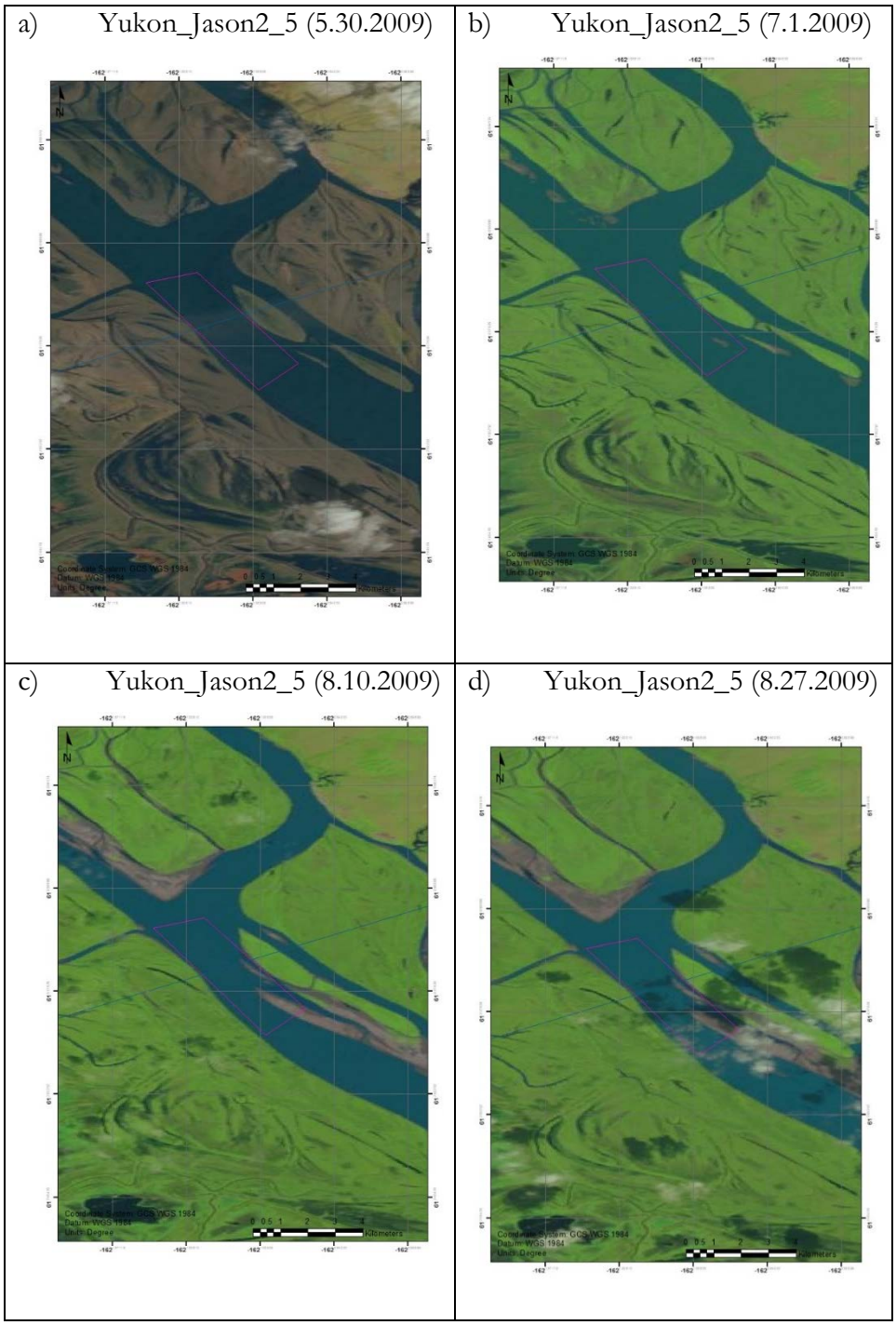

Figure A3 Landsat scenes from a) May 30 2009, b) July 1 2009, c) August 10 2009, d) August 27 2009

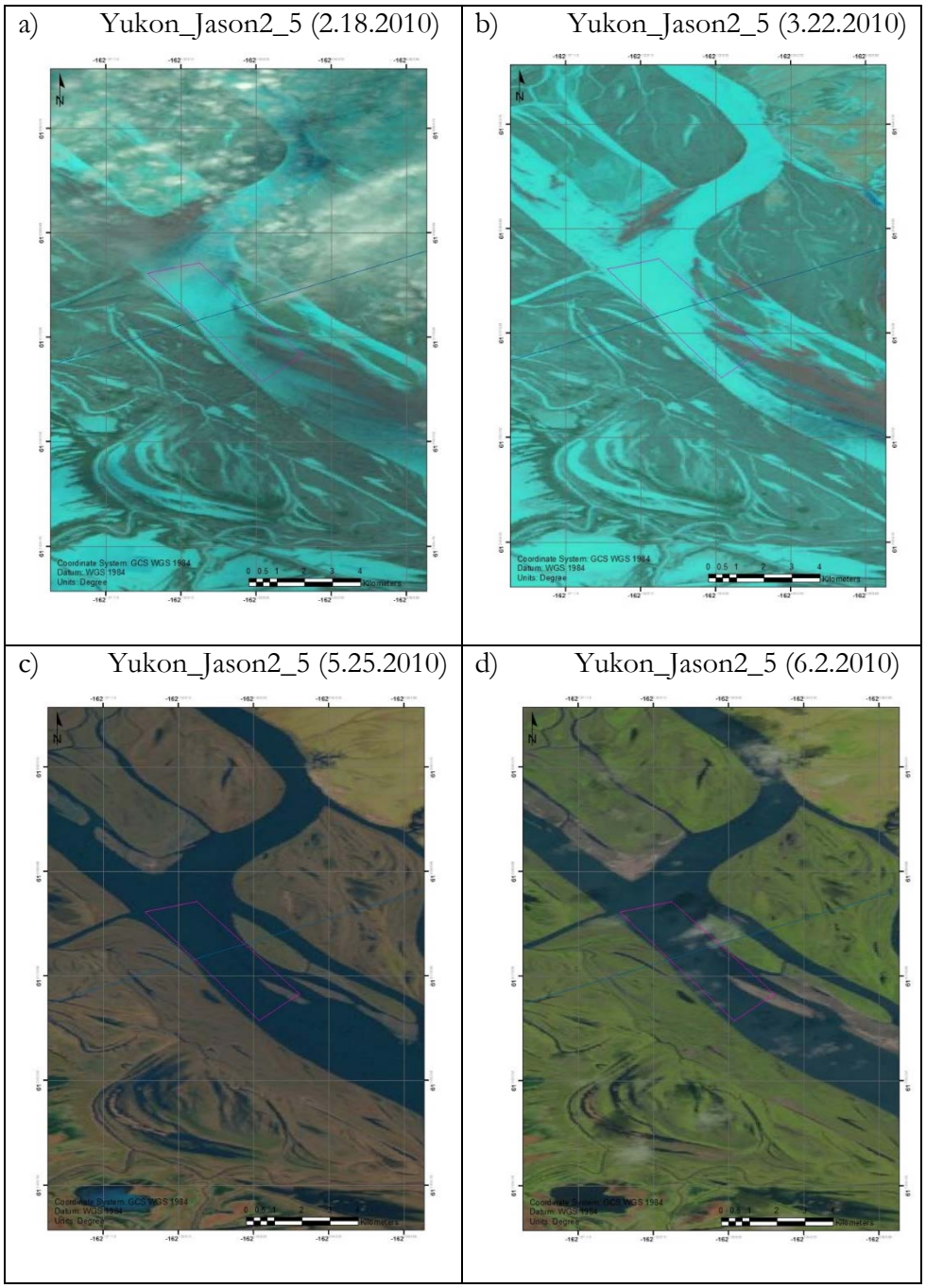

Figure A4 Landsat scenes from a) February 18 2010, b) March 22 2010, c) May 25 2010, d) June 2 2010

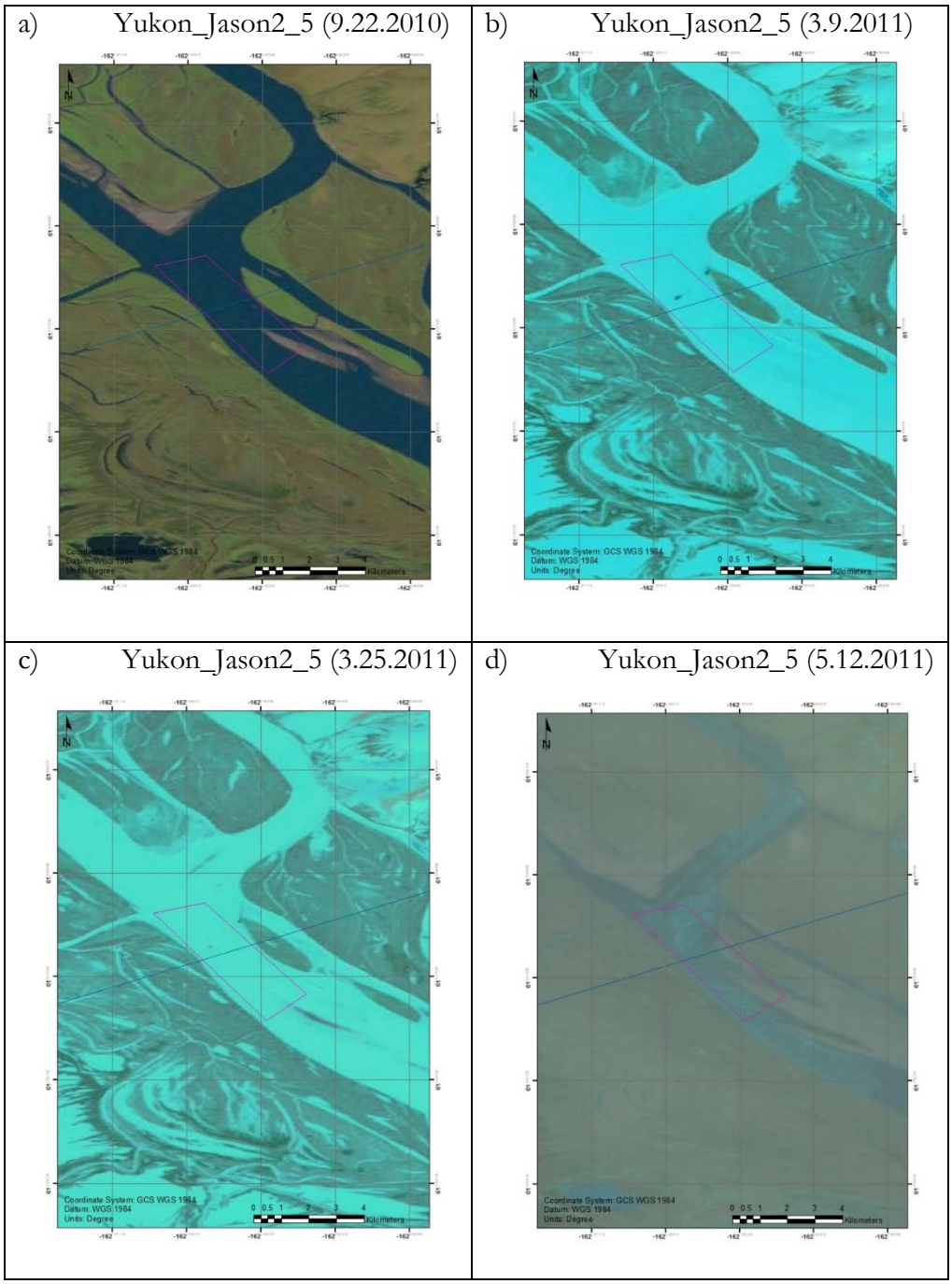

Figure A5 Landsat scenes from a) September 22 2010, b) March 9 2011, c) March 25 2011, d) May 12 2011

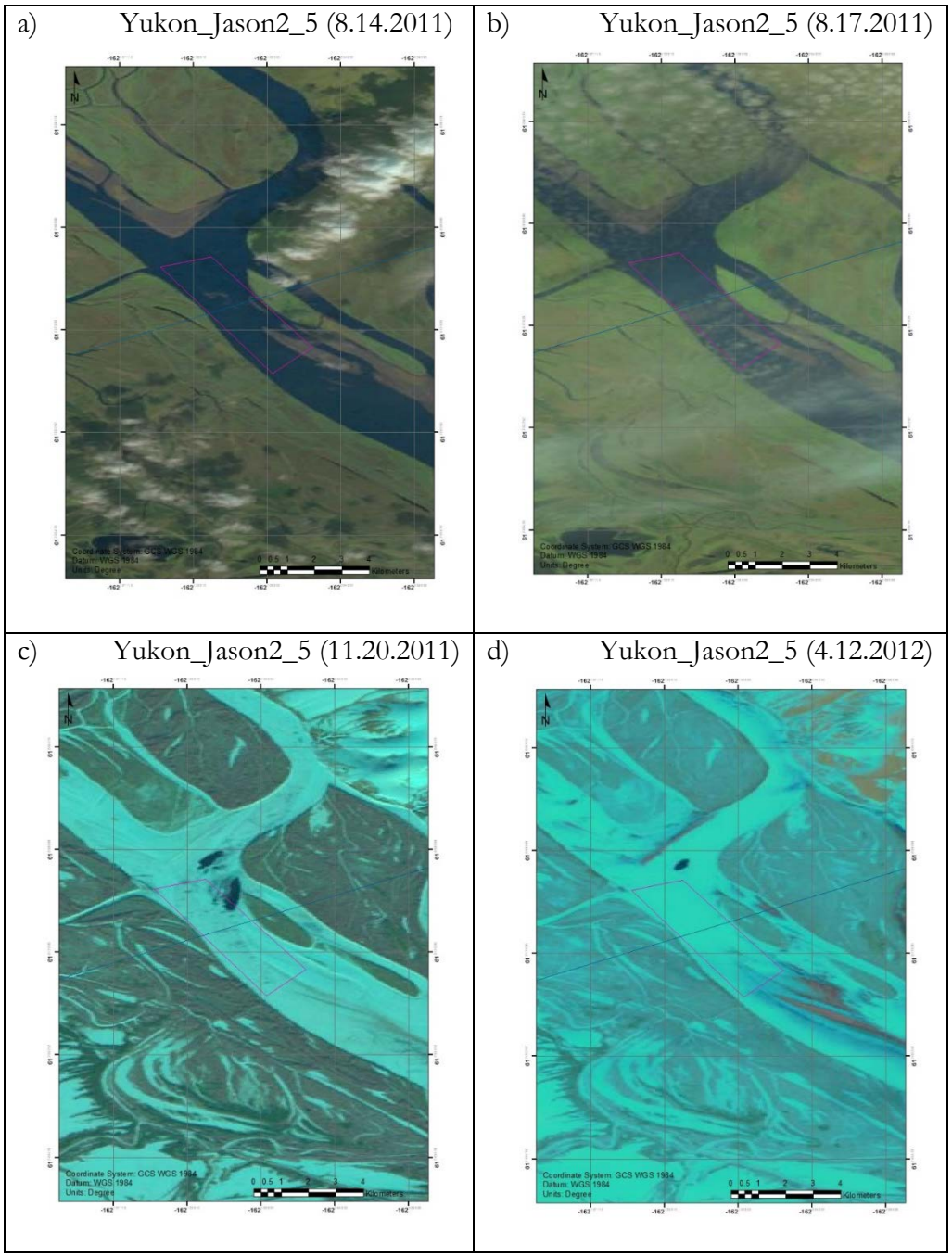

Figure A6 Landsat scenes from a) August 14 2011, b) August 17 2011, c) November 20 2011, d) April 10 2012

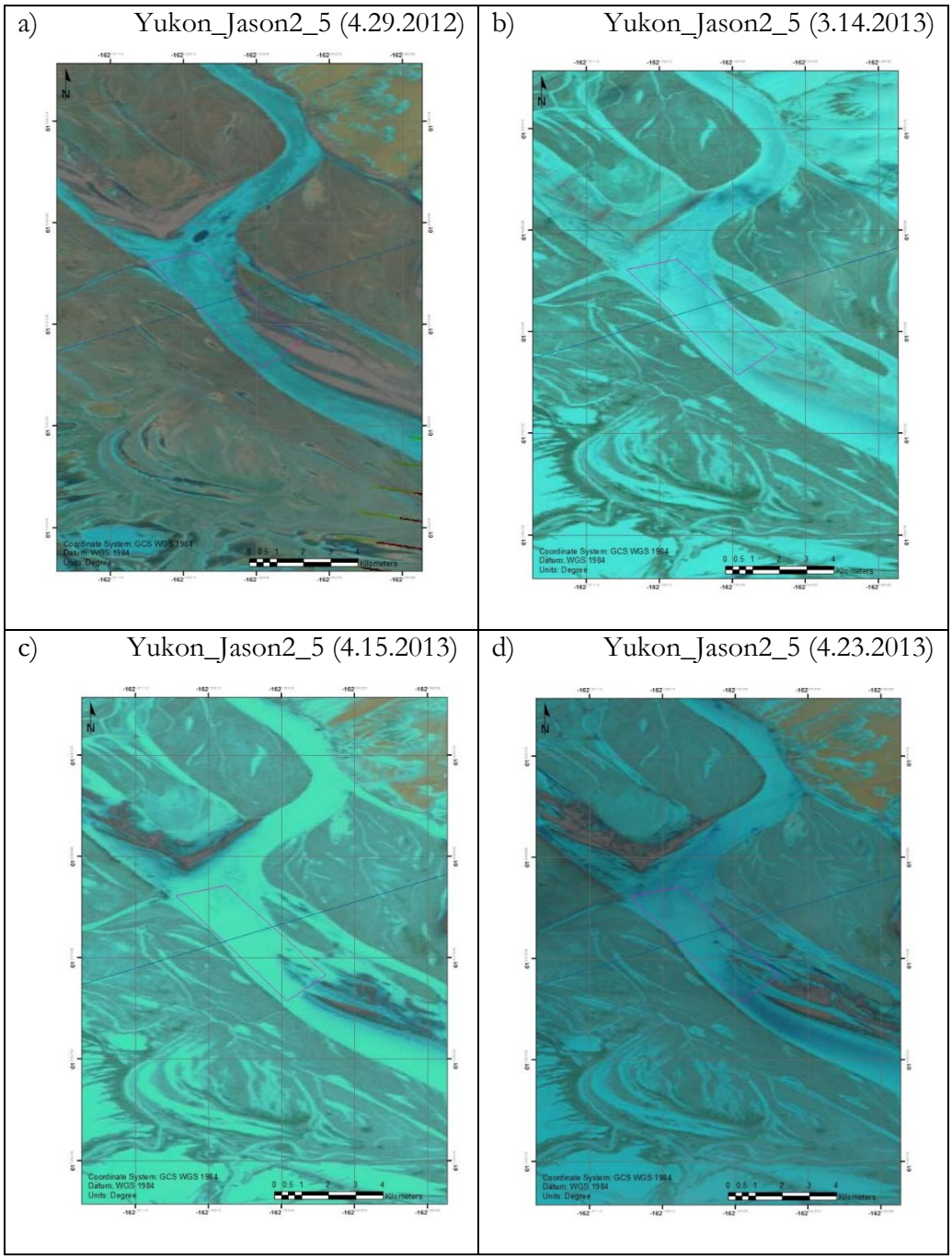

Figure A7 Landsat scenes from a) April 29 2012, b) March 14 2013, c) April 15 2013, d) April 23 2013

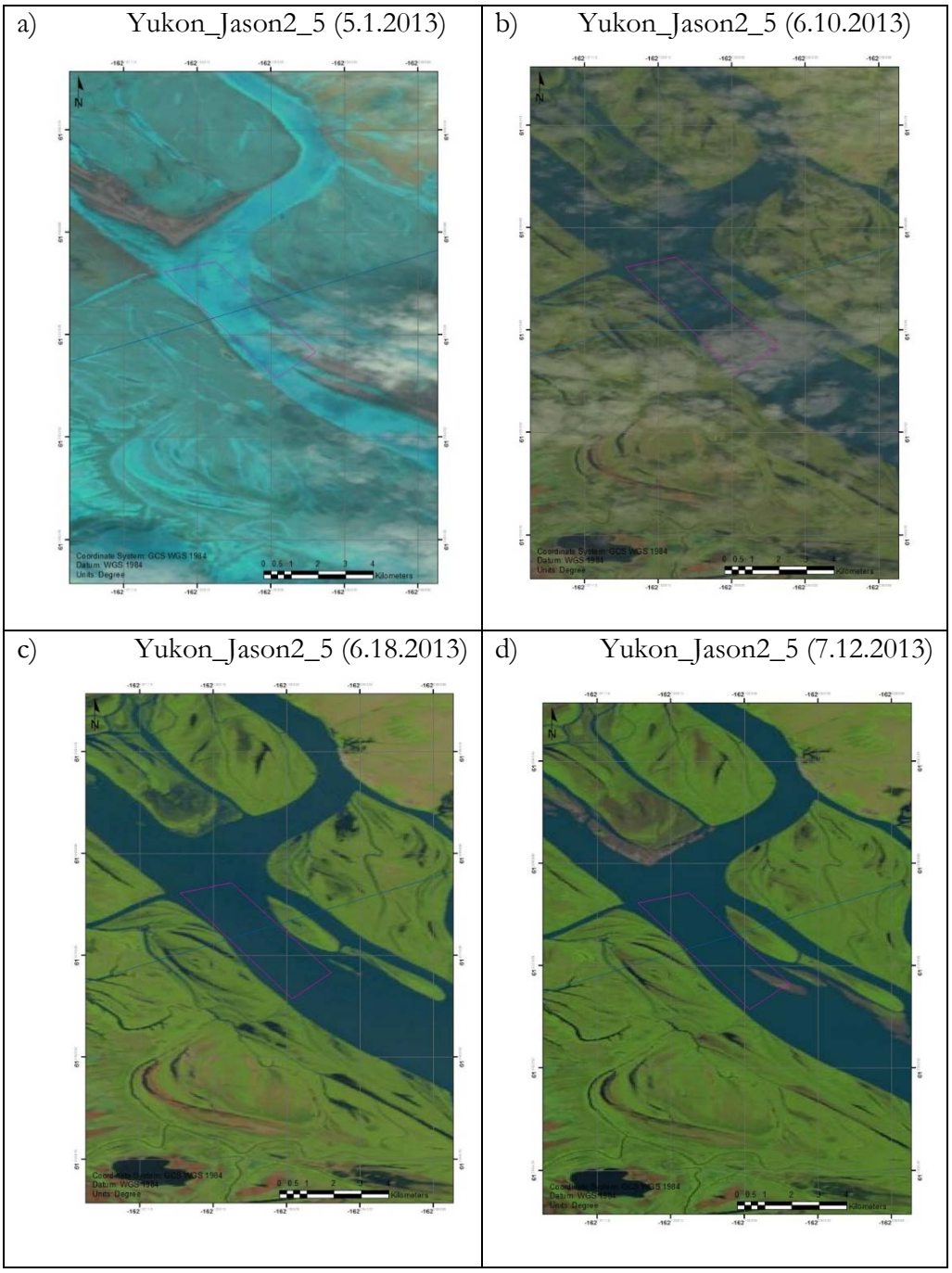

Figure A8 Landsat scenes from a) May 1 2013, b) June 10 2013, c) June 18 2013, d) July 12 2013

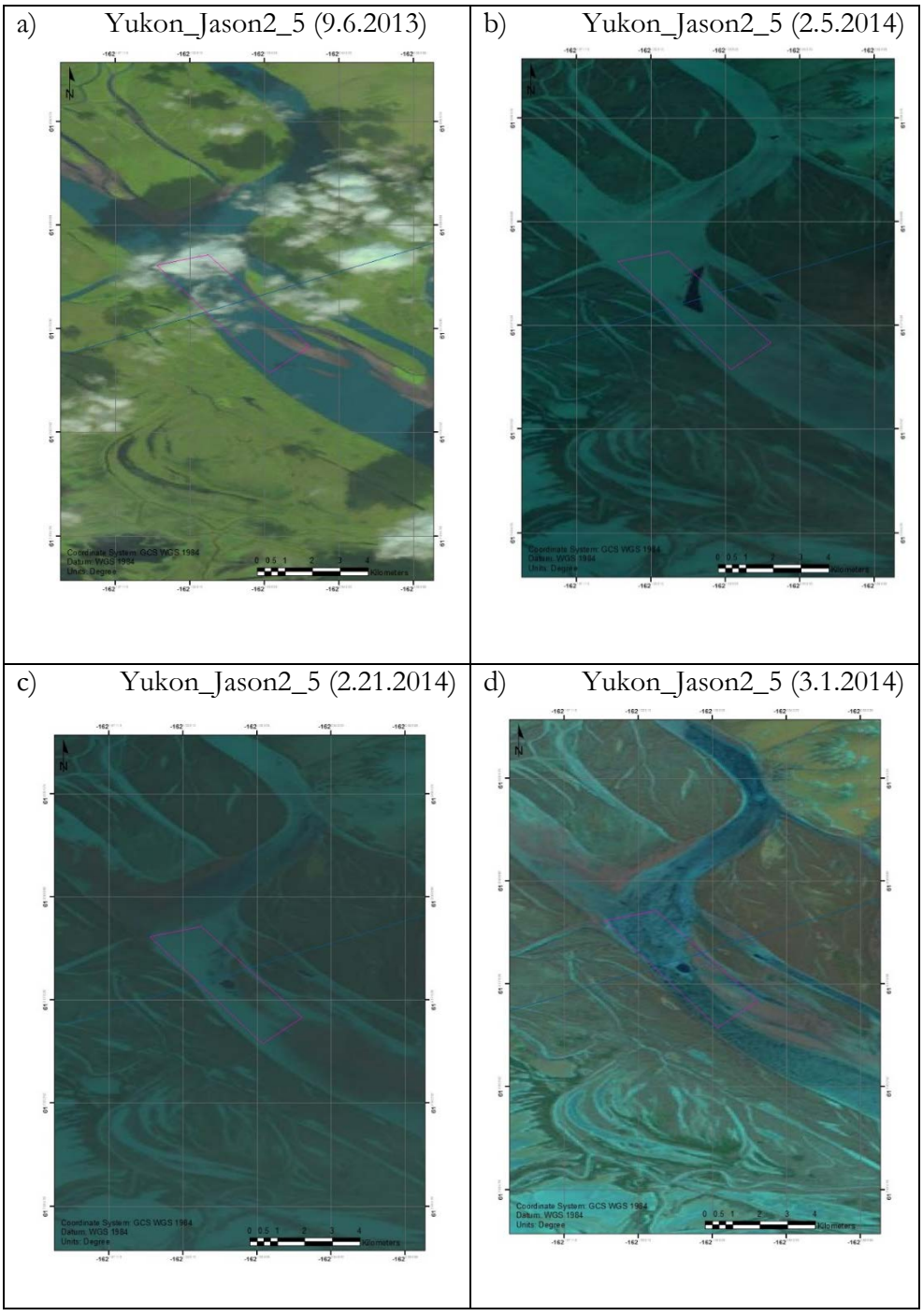

Figure A9 Landsat scenes from a) September 6 2013, b) February 5 2014, c) February 21 2014, d) March 1 2014

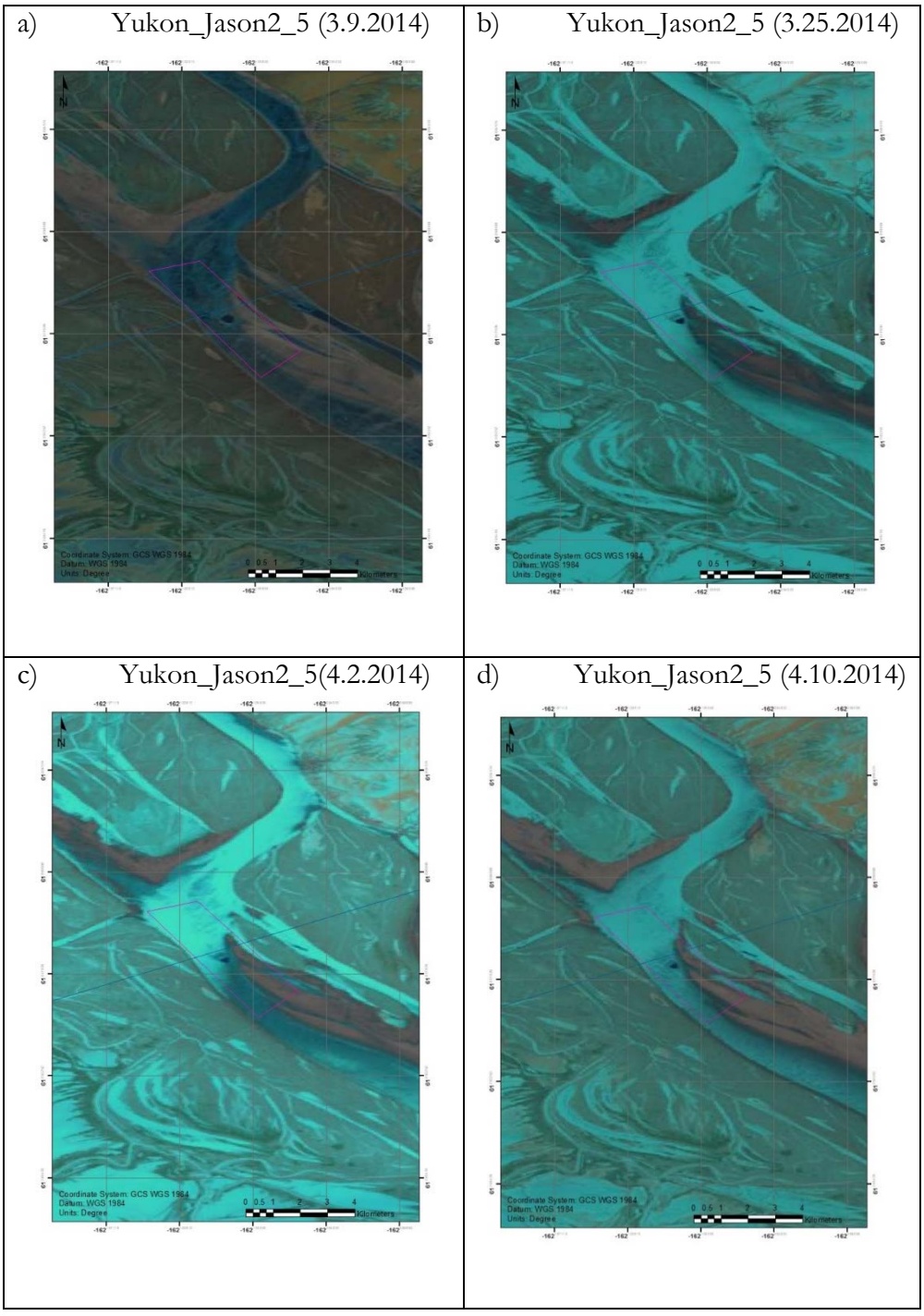

Figure A 10 Landsat scenes from a) March 9 2014, b) March 25 2014, c) April 2 2014, d) April 10 2014

a) Yukon_Jason2_5 (4.26.2014)

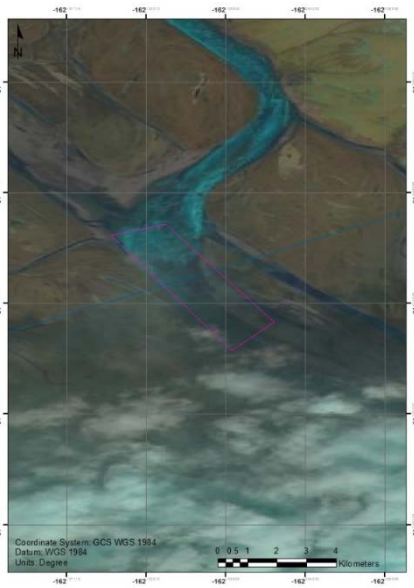

b) Yukon_Jason2_5 (5.14.2014)

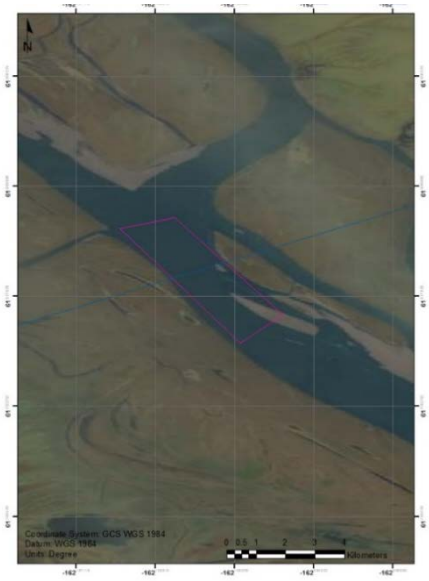

c) Yukon_Jason2_5 (6.21.2014)

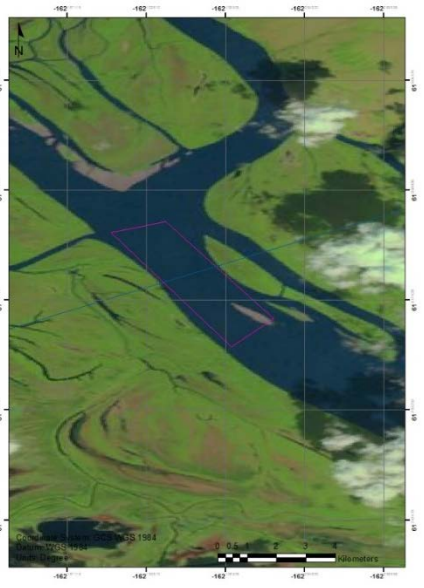

Figure A11 Landsat scenes from a) April 26 2014, b) May 14 2014, c) June 21 2014

Figure Number	Landsat Date	USGS Height [m]	Jason-2 Date	Jason-2 average height [m] Above EGM 2008 Geoid	Jason-2 average σ_0 [dB]
A1.a	7 July 2008	5.91	No data	No data	No data
A1.b	24 August 2008	6.02	Height filter	Height filter	Height filter
A1.c	26 October 2008	Not reported	Month of offset	Month of offset	Month of offset
A1.d	19 March 2009	Not reported	Month of offset	Month of offset	Month of offset
A2.a	4 April 2009	Not reported	6 April 2009	5.24	13.18
A2.b	20 April 2009	Not reported	16 April 2009	7.59	12.25
A2.c	6 May 2009	Not reported	6 May 2009	6.83	33.15
A2.d	14 May 2009	6.10	16 May 2009	7.60	42.44
A3.a	30 May 2009	8.13	26 May 2009	9.46	30.50
A3.b	I July 2009	7.17	4 July 2009	7.75	49.04
A3.c	10 August 2009	Not reported	13 August 2009	7.25	25.30
A3.d	27 August 2009	4.18	23 August 2009	4.21	37.92
A4.a	18 February 2010	Not reported	17 February 2010	2.40	19.57
A4.b	22 March 2010	Not reported	19 March 2010	3.21	20.18
A4.c	25 May 2010	7.49	28 May 2010	6.61	42.79
A4.d	2 June 2010	5.40	28 May 2010	6.14	51.62
A5.a	22 September 2010	5.297	24 September 2010	6.68	29.41
A5.b	9 March 2011	Not reported	11 March 2011	3.25	15.06
A5.c	25 March 2011	Not reported	21 March 2011	.72	17.71

A5.d	12 May 2011	Not reported	10 May 2011	2.26	33.46
A6.a	14 August 2011	6.61	17 August 2011	7.30	27.93
A6.b	17 August 2011	6.61	17 August 2011	7.30	27.93
A6.c	20 November 2011	Not reported	No data	No data	No data
A6.d	12 April 2012	Not reported	11 April 2012	.91	26.5
A7.a	29 April 2012	Not reported	1 May 2012	9.43	24.06
A7.b	14 March 2013	Not reported	14 March 2013	3.62	21.27
A7.c	15 April 2013	Not reported	No data	No data	No data
A7.d	23 April 2013	Not reported	23 April 2013	5.82	29.74
A8.a	1 May 2013	Not reported	23 April 2013	5.82	29.74
A8.b	10 June 2013	8.35	11 June 2013	9.18	30.32
A8.c	18 June 2013	8.39	21 June 2013	9.37	51.01
A8.d	12 July 2013	6.57	11 July 2013	6.98	37.31
A9.a	6 September 2013	5.46	30 August 2013	5.58	30.93
A9.b	5 February 2014	Not reported	4 February 2014	2.49	34.89
A9.c	21 February 2014	Not reported	24 February 2014	2.16	32.25
A9.d	1 March 2014	Not reported	24 February 2014	2.16	32.25
A10.a	9 March2014	Not reported	16 March 2014	1.75	28.20
A10.b	25 March 2014	Not reported	16 March 2014	1.75	28.20
A10.c	2 April 2014	Not reported	5 April 2014	1.40	36.50
A10.d	10 April 2014	Not reported	5 April 2014	1.40	36.50

A11.a	26 April 2014	Not reported	24 April 2014	2.29	42.96
A11.b	14 May 2014	5.96	14 May 2014	7.06	49.04
A11.c	21 June 2014	6.7544	14 June 2014	7.02	32.03

Table A1 Data from preceding Images

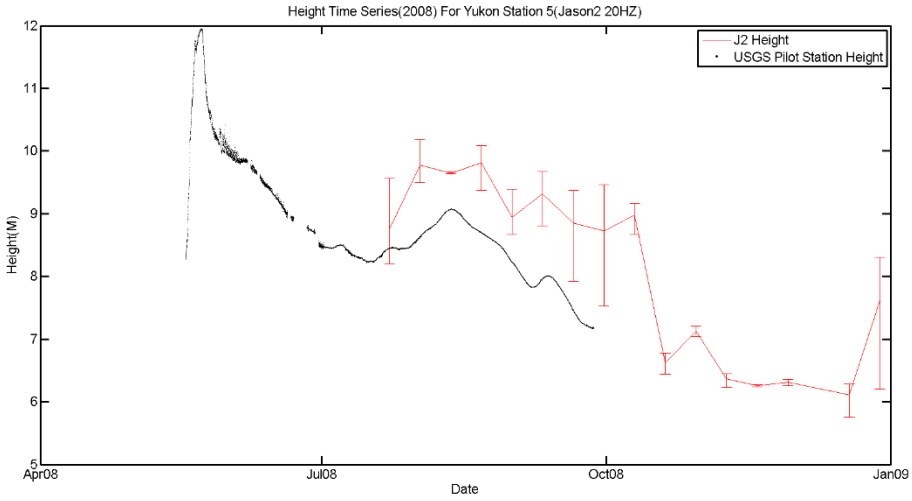

Figure A12 Height time series for Yukon station 5 (2008)

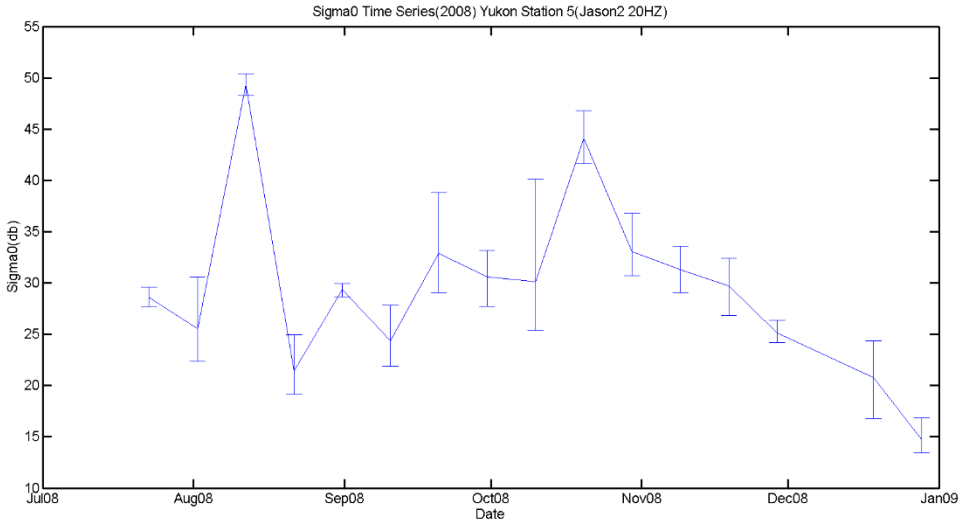

Figure A13 σ_0 Time series for Yukon station 5 (2008)

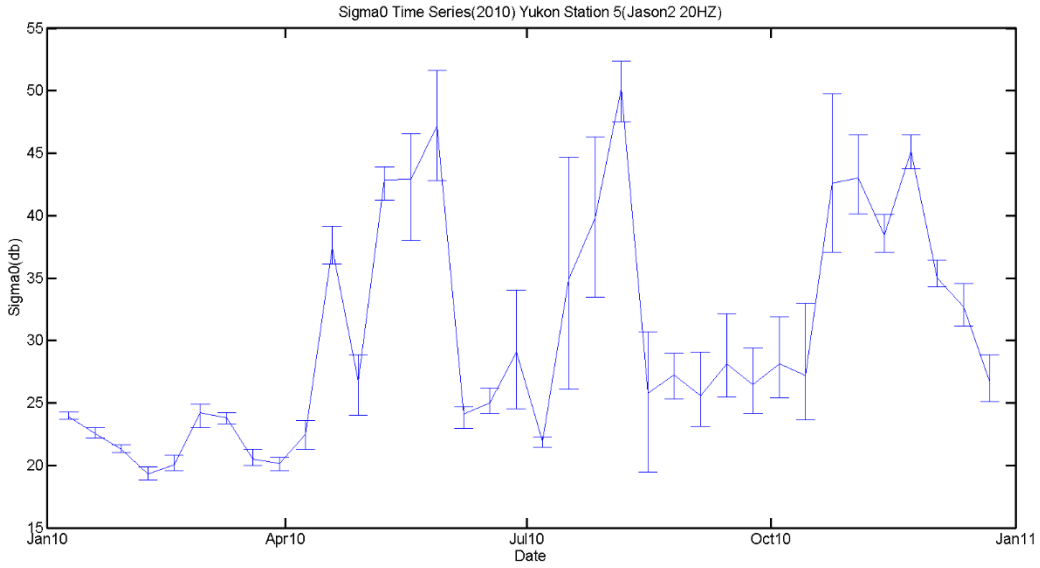

Figure A15 σ_0 Time series for Yukon station 5 (2010)

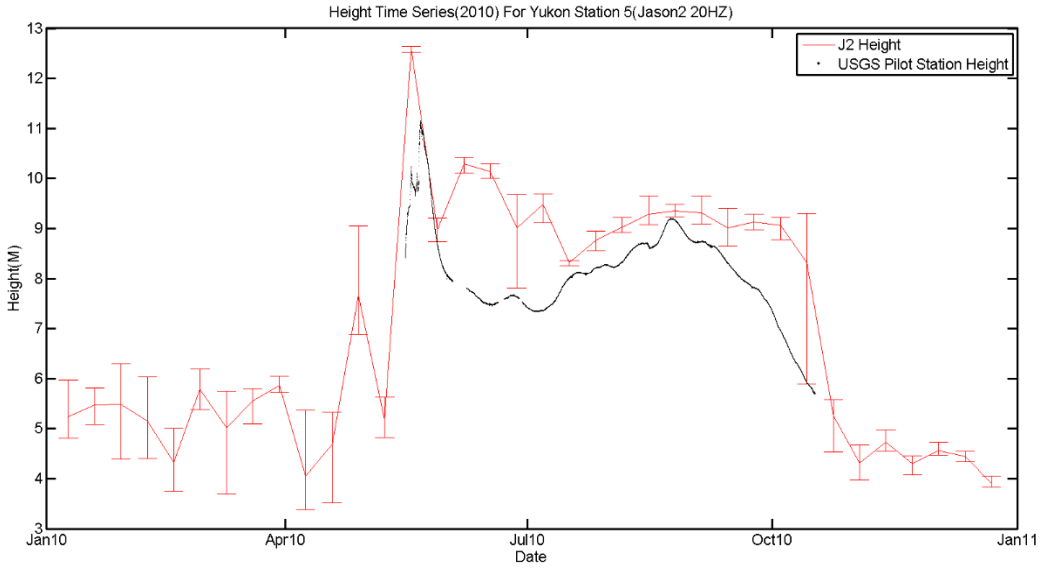

Figure A14 Height Time series for Yukon station 5 (2010)

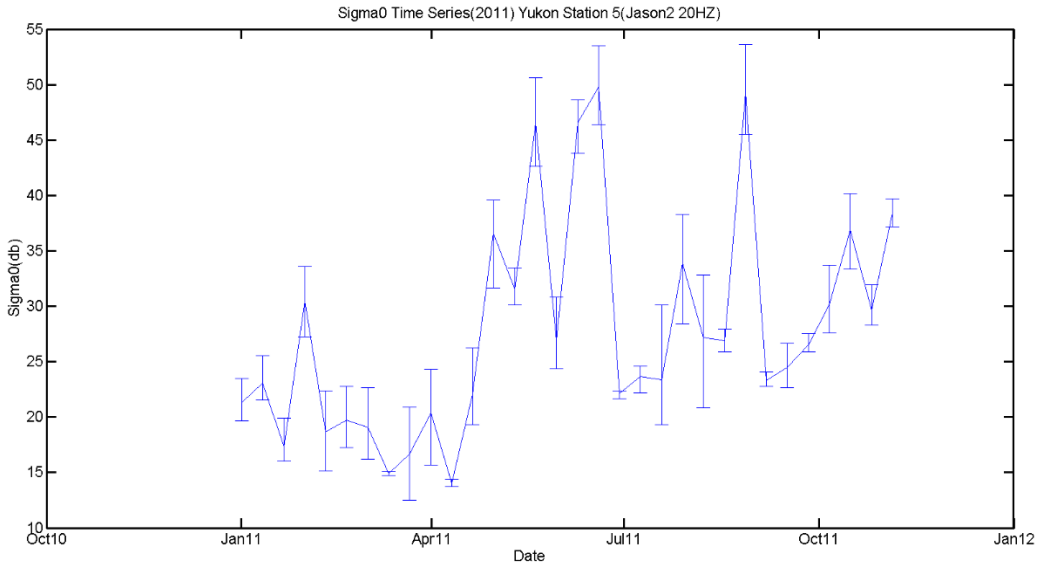

Figure A16 σ_0 Time series for Yukon station 5 (2011)

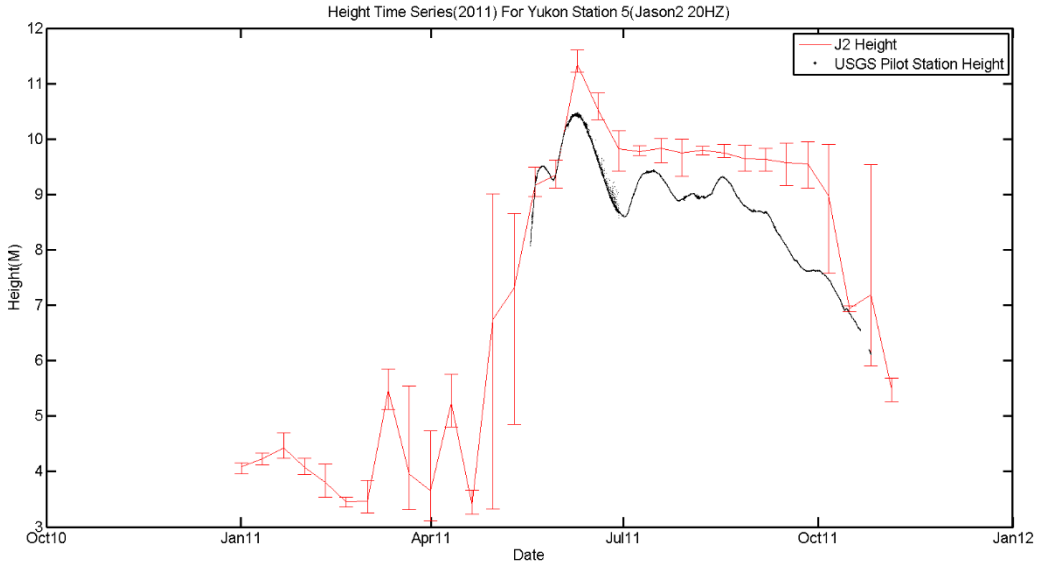

Figure A17 Height Time series for Yukon station 5 (2011)

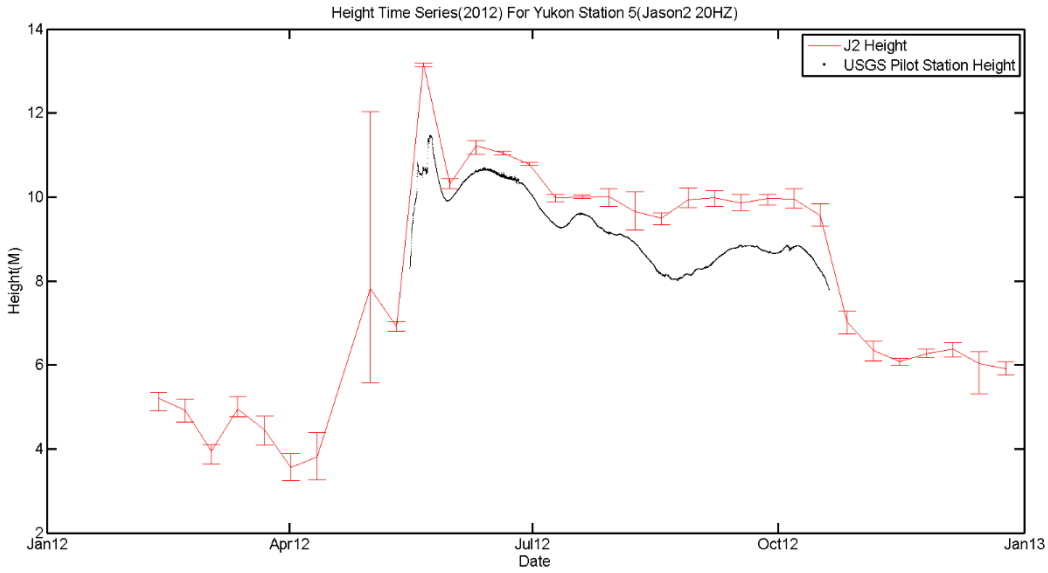

Figure A18 Height Time series for Yukon station 5 (2012)

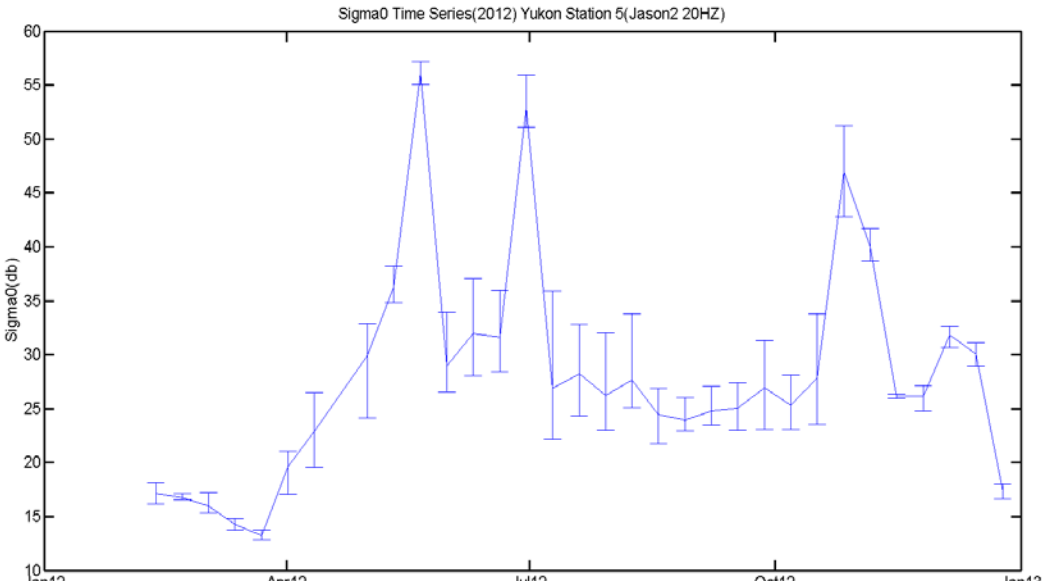

Figure A 19 σ_0 Time series for Yukon station 5 (2012)

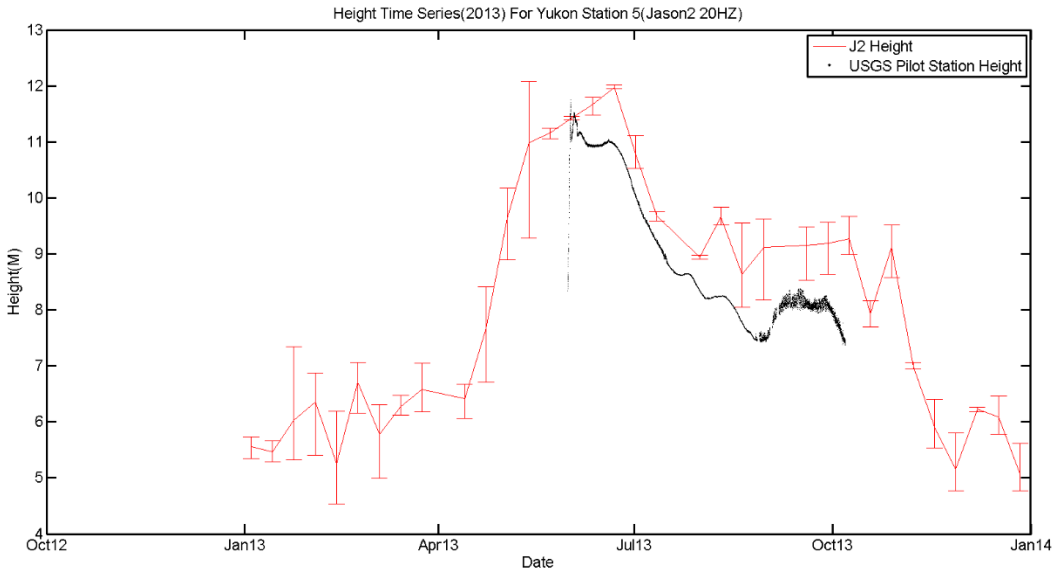

Figure A20 Height Time series for Yukon station 5 (2013)

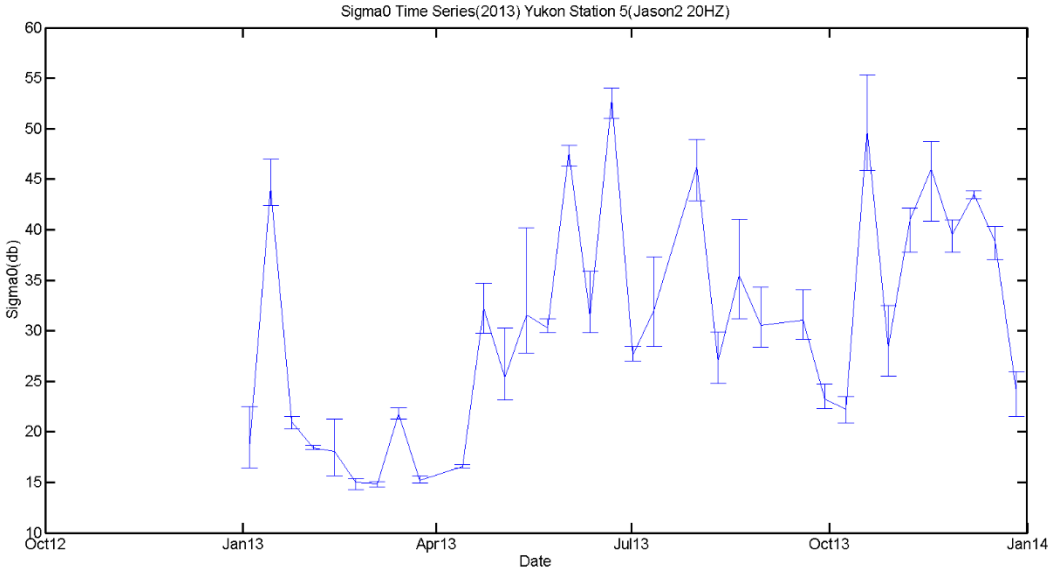

Figure A21 σ_0 Time series for Yukon station 5 (2013)

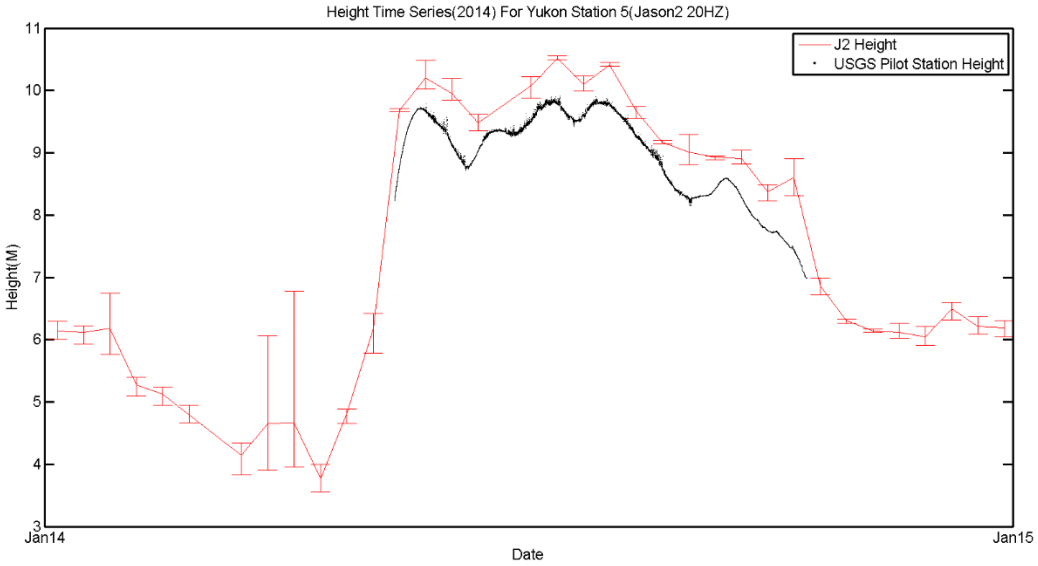

Figure A22 Height Time series for Yukon station 5 (2014)

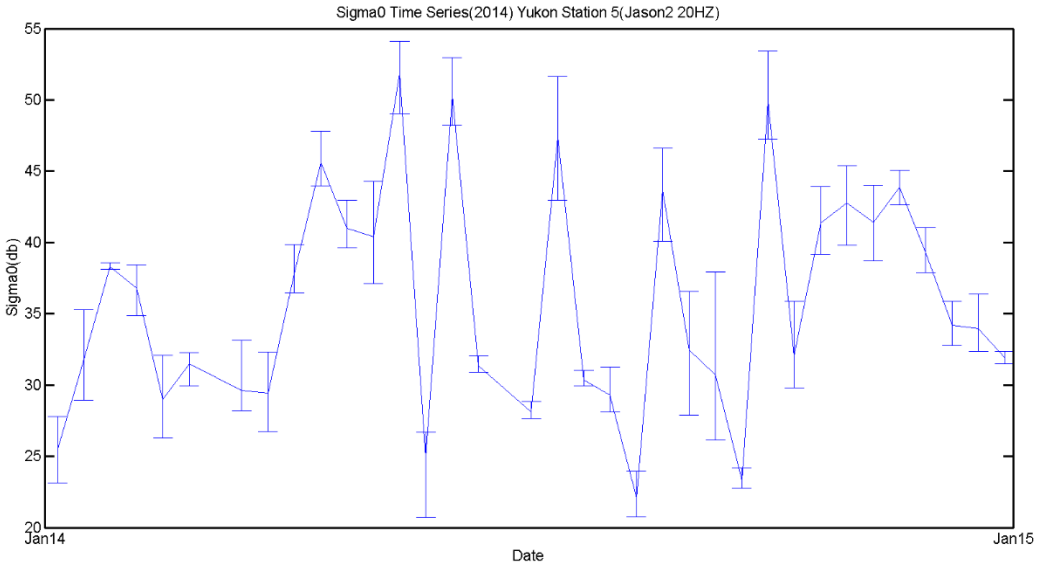

Figure A 23 σ_0 Time series for Yukon station 5 (2014)